REPORT DOCUMENTATION PAGE

Form Approved
OMB No. 0704-0188

PLEASE DO NOT RETURN YOUR FORM TO THE ABOVE ADDRESS.

1. REPORT DATE *(DD-MM-YYYY)*	2. REPORT TYPE	3. DATES COVERED *(From - To)*
resubmitted 13 Sept 2012	Final Technical	15 Mar 2008 to 30 Nov 2011

4. TITLE AND SUBTITLE
DPN-Generated Combinatorial Libraries

5a. CONTRACT NUMBER

5b. GRANT NUMBER
FA9550-08-1-0124

5c. PROGRAM ELEMENT NUMBER

6. AUTHOR(S)
Chad Mirkin

5d. PROJECT NUMBER

5e. TASK NUMBER

5f. WORK UNIT NUMBER

7. PERFORMING ORGANIZATION NAME(S) AND ADDRESS(ES)
Northwestern University

8. PERFORMING ORGANIZATION REPORT NUMBER

9. SPONSORING/MONITORING AGENCY NAME(S) AND ADDRESS(ES)
AFOSR
875 N. Randolph St
Arlington, VA 22203

10. SPONSOR/MONITOR'S ACRONYM(S)

11. SPONSOR/MONITOR'S REPORT NUMBER(S)
AFRL-OSR-VA-TR-2012-1084

12. DISTRIBUTION/AVAILABILITY STATEMENT
Distribution A: Approved for Public Release

13. SUPPLEMENTARY NOTES

14. ABSTRACT

Here, we summarize the accomplishments relating to generating combinatorial libraries using dip-pen nanolithography (DPN) that we achieved during this AFOSR grant. Through powerful technological advances, we were able to meet the aims laid out in the proposal. Our first objective was to universally control the transport of matter at the nanoscale to improve the capabilities of DPN. To this end, we performed a systematic study to understand the dynamics of ink transport while developing agarose- and matrix-assisted DPN for the deposition of arbitrary materials. We achieved our next goal – individually inking pens in order to write patterns with multiple inks at once – by directly depositing ink in a self-correcting manner onto individual pens via ink-jet printing. Our final objective was to synthesize combinatorial arrays on a surface for biological screening, and we have made great progress towards this by developing massively

15. SUBJECT TERMS

16. SECURITY CLASSIFICATION OF:			17. LIMITATION OF ABSTRACT	18. NUMBER OF PAGES	19a. NAME OF RESPONSIBLE PERSON
a. REPORT	b. ABSTRACT	c. THIS PAGE			Chad Mirkin
unclassified	unclassified	unclassified	unclassified (U)		19b. TELEPHONE NUMBER *(Include area code)* 847-491-2907

AFOSR Final Report

DPN-Generated Combinatorial Libraries

Grant Number: FA9550-08-1-0124

Principal Investigator:
Chad A. Mirkin
chadnano@northwestern.edu
Phone: 847-491-2907
Fax: 847-467-5123

Department of Chemistry
Northwestern University
2145 Sheridan Road
Evanston, IL 60208

February 29, 2012

Period covered by this report:
3/15/08 to 11/30/11

Abstract

Here, we summarize the accomplishments relating to generating combinatorial libraries using dip-pen nanolithography (DPN) that we achieved during this AFOSR grant. Through powerful technological advances, we were able to meet the aims laid out in the proposal. Our first objective was to universally control the transport of matter at the nanoscale to improve the capabilities of DPN. To this end, we performed a systematic study to understand the dynamics of ink transport while developing agarose- and matrix-assisted DPN for the deposition of arbitrary materials. We achieved our next goal – individually inking pens in order to write patterns with multiple inks at once – by directly depositing ink in a self-correcting manner onto individual pens via ink-jet printing. Our final objective was to synthesize combinatorial arrays on a surface for biological screening, and we have made great progress towards this by developing massively parallel cantilever-free scanning probe lithography techniques (polymer pen lithography, hard-tip soft-spring lithography) that enabled the creation of combinatorial arrays of biomolecules with defined feature size and demonstrated their utility in studying cell differentiation. Furthermore, we developed a method to generate combinatorial arrays of sub-5 nm single crystal nanoparticles that act as binding sites for single proteins or as catalysts.

A.1 Introduction

This section summarizes the research accomplished under this grant. It is separated into subsections that are defined by the proposed objective that the work addresses. The objectives of this grant were: (1) To develop universal ink materials capable of controlling the transport of various materials from a scanning probe tip to a surface of interest and understand their transport properties. Such "universal inks" could be used for patterning many desired materials in a manner that is independent of material composition, molecular weight, charge, and viscosity, among other diffusion-related properties. We have completely addressed this goal through the development of agarose- and matrix-assisted DPN, as is discussed in Section A.2. (2) To develop methods for individually addressing AFM tips with different inks and directly pattern multi-component arrays using the universal ink carriers, which would enable the synthesis of complex nanoarrays comprised of biomolecules. This goal was addressed through the development of ink-jet printing cantilevers and pens in cantilever-free arrays, as discussed in Section A.3. (3) To develop a DPN-based nanoscale oligonucleotide synthetic method for constructing combinatorial libraries of DNA at the nanometer length scale. Throughout the course of this grant, we have shifted objective 3 to focus on using scanning probed-based tools to generate combinatorial libraries of extracellular matrix proteins, which we used to probe mesenchymal stem cell differentiation (Section A.4). In addition to the synthesizing combinatorial libraries for studying stem-cell differentiation, we developed of versatile and robust methods for large area nanoscale patterning. These enabling developments are highlighted in Section A.4, where we outline several massively parallel techniques for generating large-scale combinatorial arrays of single crystal nanoparticles for catalysis and immobilizing individual proteins.

A.2. Universal Control of Ink Transport

Transport Model for DPN

The proposed mechanisms of DPN ink-transport involves the movement of ink molecules to a surface through a water meniscus formed between an AFM tip and the substrate. More specifically, DPN transport models typically assume that the tip which is coated with an

alkanethiol (e.g., mercaptohexadecanoic acid (MHA)) is a point source of constant concentration or flux. Although a constant point source model explains the time-dependent growth of MHA patterns for a single ink-coated tip, the variation of transport rates among different tips or for different ink coating methods has been ignored, despite its importance to forming a complete understanding of material transport. Such an understanding would allow one to significantly increase the reproducibility of DPN and aid in parallelization efforts, where one must be able to achieve uniform and nearly identical transport rates from different pens in an array.

To address this problem, inkjet printing was used to precisely control the number of molecules inked on the AFM tips that were subsequently used to create patterns. From these experiments, a quantitative model was derived that accounted for the variation in DPN transport rate and a method for diminishing this variation. Using a non-contact inkjet printer, 7-pen Si_xN_y cantilever arrays with a 150 μm pen-to-pen spacing were inked using one to seven 320 pL droplets of a 10 mM MHA-ethanol solution. These inked pens were subsequently used to generate MHA self-assembled monolayer (SAM) patterns on Au substrates (Figure 1) that were imaged by tapping mode AFM. These experiments demonstrated for each set of droplets a linear dependence of the dot feature areas on dwell time (Fig. 2). These functions match the previous contact point source theory. Importantly, it was found that the ink transport rate is a function of the amount of material deposited on a pen and can be systematically adjusted on the basis of the number of ink droplets delivered. For pens inked with up to seven droplets, the transport rate increased nonlinearly with the number of droplets followed by saturation (Fig. 2).

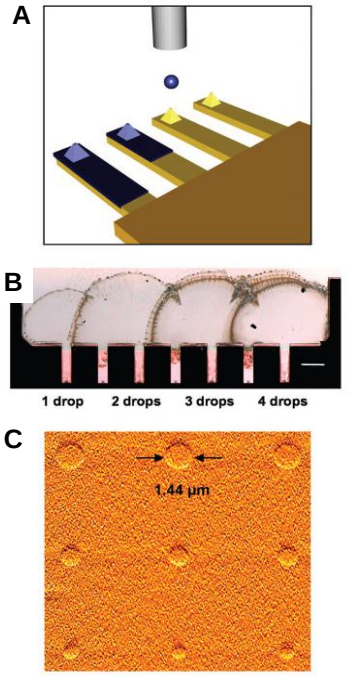

Figure 1. *(A) Scheme of an inkjet printer addressing individual tips in a cantilever array. (B) Optical microscopy image of Si_xN_y cantilevers inked with an increasing number of drops of 10 mM ethanolic mercaptohexadecanoic acid (MHA) solution. (C) Representative error signal image (scan rate 4 Hz) of dot features formed at 24°C and a relative humidity (RH) of 45 ±3% on fresh Au surfaces by a tip inked with 5 drops of MHA-ethanol. From top to bottom, contact times are 16, 8, and 4 s, respectively.*

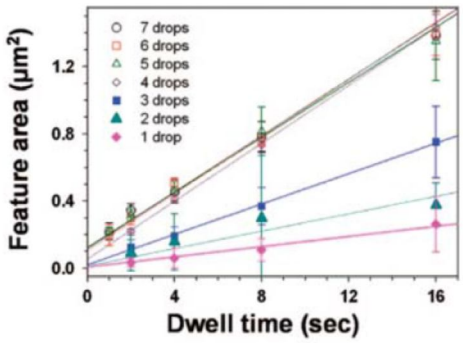

Figure 2*. MHA dot areas measured as a function of dwell time for tips inked with an increasing number of drops of 10 mM MHA-ethanol. All experiments were conducted at 24°C at a RH of 45% on fresh Au substrates. For each set of inked tips, the relationship* $P \propto Dt + b$ *can be used where P is the feature area, D is the transport rate, t is the dwell time, and b is the effective tip area in contact with the meniscus.*

It was further demonstrated that the mass-dependent ink transport rates are neither the result of an increase in the tip radius of curvature or residual solvent as more ink is delivered to the tip. The intersection of the y-axis in the plot of feature size vs. dwell time (Fig. 2) corresponds to the tip radius, suggesting that there is a minimal increase in tip radius as more ink is added. The increased transport rate is not due to residual solvent either because the transport rates of the inked tips with and without vacuum treatment (~10^{-2} Torr, 18 hours) were the same. The observation of mass-dependent ink transport rates arises from the rapid depletion of MHA from the water meniscus. To form a dot feature with a diameter of 1.4 μm in 16 s, more than 7.5 x 10^6 molecules are necessary, based on an MHA footprint of 0.229 nm^2, far exceeding the number of MHA molecules dissolved in a saturated meniscus (~70 molecules, on the basis of the meniscus volume at a relative humidity of 40%). These values correspond to an average flux of over 3.8 ×10^5 molecules s^{-1} and indicate a high concentration gradient within the meniscus. Since the rate of MHA adsorption to a gold surface at 300K is relatively fast at ~1.0 ×10^3 M^{-1} sec-1, it can be concluded that the limiting step in the transport process occurs at the tip, the source of MHA.

To better understand the origin of mass-dependent transport rates, droplets of a 10 mM MHA in ethanol solution were deposited on a flat Si_xN_y surface near the cantilevers and the surface topology measured by AFM. Instead of a complete and homogeneous coating of MHA on the substrate, crystallites were observed. The dependence of ink surface coverage on the number of MHA-ethanol droplets for flat Si_xN_y substrates translates to a linear relationship between the observed MHA transport rates and the surface area of the ink (Fig. 3). Unlike previous transport models for DPN, which account for constant concentration or flux of MHA, surface-area dependent dissolution of material from the tip controls the transport rate. In such settings, the effect of material solubility on dissolution is negligible because the system is far from saturation; the limiting factor controlling feature size is the surface area of the material, rather than its solubility. The rate of dissolution at the tip can be defined as:

$$\frac{dx}{dt} = \left(\frac{dN}{dt}\right)_{\text{detach}} - \left(\frac{dN}{dt}\right)_{\text{attach}} = \frac{b}{\pi a^2} v e^{-E_D/kT} - b\left(\frac{kT}{2\pi m}\right)^{1/2} e^{-E_A/kT} C_0$$

where N is the number of molecules, b is the effective contact area between MHA on the tip and the meniscus, πa^2 is the footprint area of MHA (0.229 nm^2), v is the effective molecule dissolution attempt frequency, k is Boltzmann's constant, T is temperature, m is the mass of one

MHA molecule (3.79×10^{-22} g), C_0 is the MHA concentration next to the tip ($<10^{-7}$), E_D is the activation energy for molecule detachment (0.467 eV per molecule), and E_A is the activation energy for attachment (0.13 eV per molecule). Values for the attempt frequency, v, of MHA dissolution were previously unavailable except through model estimations. By using measured transport rates from the DPN experiments and surface coverage values, attempt frequencies for molecule detachment can be determined. It was found that the attempt frequencies of MHA dissolution range from 1.33×10^9 to 4.42×10^9 Hz.

In conclusion, droplet-dependent MHA deposition rates are governed by the surface area of the tip covered by ink. This finding explains the large variation in transport rates associated with pens inked by dip-coating or inkwells and attributes the variation to inhomogeneous ink distribution and uneven surface coverage. The use of inkjet printing to deliver precise amounts of material to designated tips not only has enabled one to predict and tailor MHA transport rates, but it also makes DPN a more consistent and controllable nanopatterning tool. These results are the first DPN experiments that show a direct relationship between the amount of ink on a tip and the corresponding surface area with the transport rate, and they will allow controlled parallelization in nanoarrays.

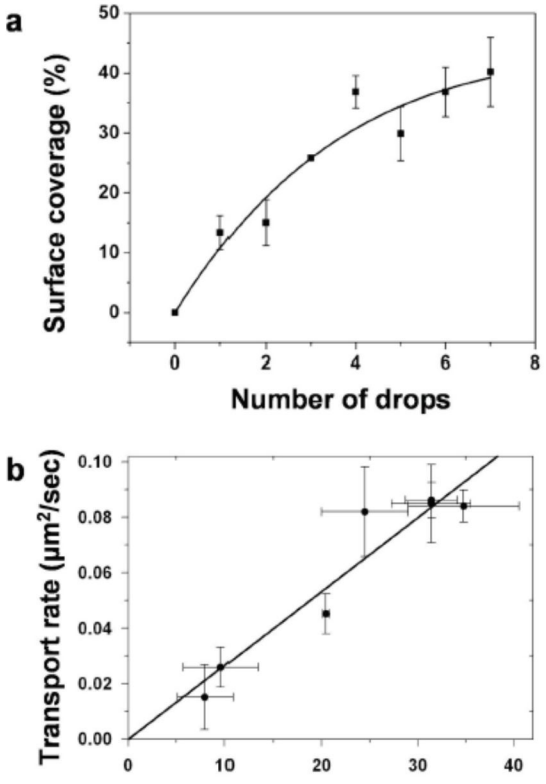

Figure 3. *(a) Surface coverage dependence on the number of MHA/ethanol drops for Si_xN_y substrates. A line was fitted using a four parameter BET equation with the constraint of passing through (0, 0). (b) MHA transport rate shows a linear dependence on the surface coverage and increases with the number of drops.*

PEG as Universal Ink Carrier

Polyethylene glycol (PEG) has been used as a universal ink carrier matrix for delivering biomolecules, proteins and inorganic nanomaterials. PEG (MW: 100,000) is an ideal matrix and has several advantageous properties which are: (1) PEG has a relatively low melting temperature

(65°C) and can be easily patterned by DPN, (2) it is soluble in many hydrophilic solvents (e.g., aqueous), which makes it a compatible ink carrier in different biological buffer solutions, (3) it can be used for patterning on a variety of substrates including SiO_x, Au, and glass, and (4) PEG is chemically inert and reacts neither with the biomolecues nor does it affect their chemical or physical properties during deposition.

We first monitored the ink diffusion rate change of the mixture of anti-ubiquitin antibody and PEG at different ratios (Fig. 4). At an anti-ubiquitin:PEG ratio of 1:2 w/w, the diffusion rate of the mixed ink jumped from 11.30 nm/s (for pure anti-ubiquitin) to 28.72 nm/s, and it increased to 29.41 nm/s at a 1:5 ratio. The ratio of PEG to protein is a critical parameter that facilitates the precise control of each ink's final feature size in DPN experiments. We then compared the transport rate of two composite inks containing fluorescent labeled BSA (green color) and anti-ubiquitin (red color) at a ratio of 1:5 for both, BSA:PEG and anti-ubiquitin:PEG. The diffusion rates of the two inks were very similar (Fig. 4). For example, at a tip-substrate contact time of 32 sec, the average dot diameter was 328.3 nm for BSA and 306.1 nm for antiubiquitin (less than 7% variation). For comparison, in the absence of PEG the generated dot sizes would be 284.3 nm and 223.1 nm. In order to demonstrate that the bioacitivities of the patterned biomolecules were maintained, we generated individual IgG and β-galactosidase patterns. At a tip-substrate contact time of 32 sec, the average dot diameter was 347.2 nm for IgG and 380.3 nm for β-galactosidase, with around 8% variation. Without the PEG matrix, the generated biomolecular dot sizes are 251.0 nm and 439.1 nm, respectively. We then incubated the biomolecular arrays with the respective antibodies (in buffer) followed by rinsing with fresh buffer solution. Both, anti-IgG and anti- β-galactosidase, did bind to the pregenerated dot arrays of antigen molecules, which indicates that the patterned IgG and β- galactosidase have remained bioactive.

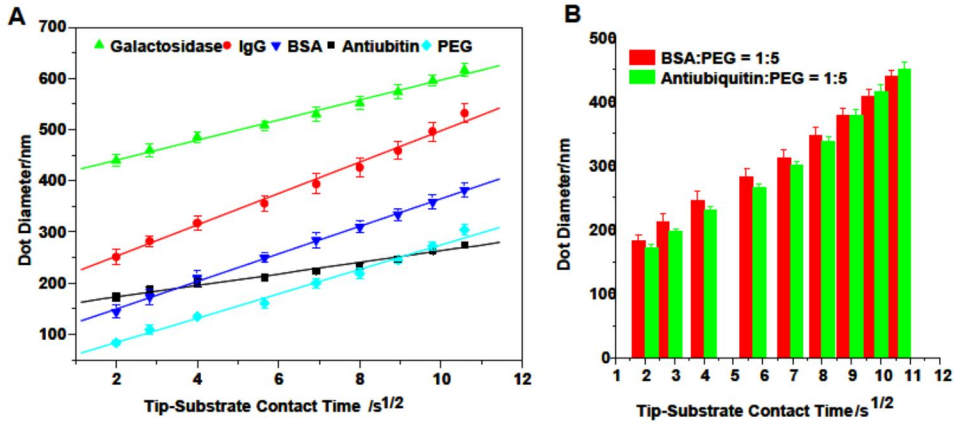

Figure 4. *(A) Plots showing the relationship of DPN-generated dot sizes with tip-substrate contact time of selected ink materials. (B) Comparison of the diffusion rate of BSA/PEG and anti-ubiquitin/PEG at a ratio of 1:5. The chart shows very similar diffusion rates.*

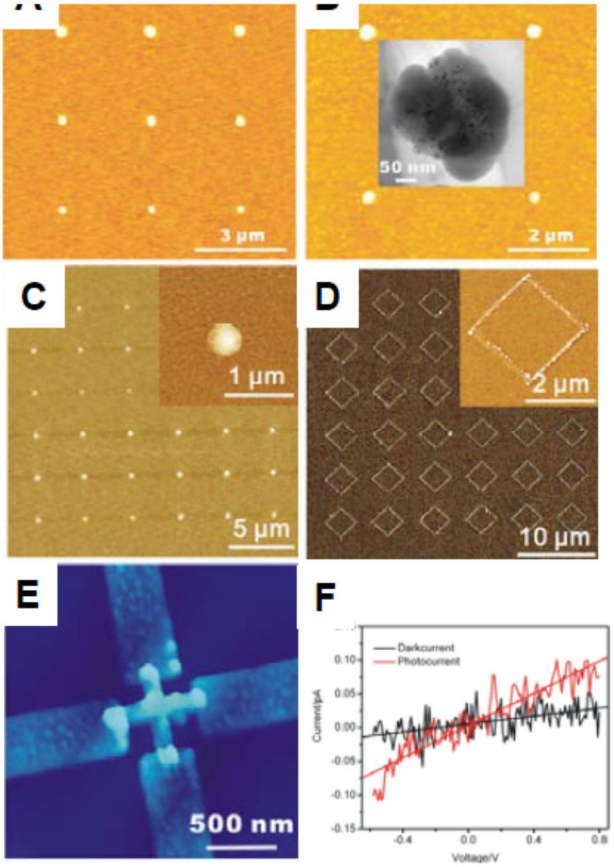

Figure 5. *Topographic AFM images of (A) a pure PEG dot array, (B) a 5 nm AuNP/PEG dot array (the inset shows a TEM image of one nanodot), (C) a 4.7 nm MNP/PEG dot array, and (D) a diamond-shaped line array. (E) DPN generated fullerene/PEG lines connecting a nanoelectrode with a 500 nm gap size. (F) I-V curves of the DPN generated transistor shown in (E), measured in dark (black line) and illuminated with a Xe (150 W) light (red line) at* 10^{-3} *torr and room temperature.*

Next, we demonstrated that these polymers can be used as ink carriers for direct patterning of nanoparticles by DPN. Figure 5 shows arrays of Au nanoparticles (AuNPs) generated by direct writing in a single-step process. In a control experiment, dot arrays of pure PEG were generated using tip-substrate contact times of 64, 32, and 16 s (Table 1); the heights of these features are 8.5, 3.3, and 1.7 nm, respectively. Table 1 clearly shows that all of the nanoscale features containing Au nanoparticles are taller compared to those that contain only PEG (Table 1). This height increase is larger for patterns containing nanoparticles of bigger diameters. The sizes of the nanopatterns can also be controlled by changing the tip-substrate contact time. When AuNP/PEG ink containing AuNPs of 5 nm was patterned on a TEM grid, clusters of AuNPs were clearly observed, which is further evidence that AuNPs were indeed patterned directly along with PEG. Patterns of magnetic nanoparticles (MNPs) were also generated using this technique. The topographic AFM images of patterned dot and line arrays (using MNP/PEO composite inks) are shown in figures 5C and 5D, respectively. Again, a clear height difference was observed compared to those that contain PEG alone and no MNPs (Table 1). The increase in height was attributed to the MNPs embedded in the DPN patterns.

Contact Time (s)	Heights of DPN-Generated Dot Features (nm)					
	Pure PEG	MNP/PEG	AuNP/PEG (2 nm)	AuNP/PEG (5 nm)	AuNP/PEG (13 nm)	C60/PEG
64	8.5	27.4	20.8	25.8	32.3	21.8
32	3.3	23.1	13.8	16.1	23.5	14.6
16	1.7	18.3	8.6	10.6	18.5	9.8

Table 1. Height profiles of DPN-generated dot features composed of pure PEG and its mixture with different nano building blocks.

In addition to AuNPs and MNPs, DPN patterns composed of the carbon-based nanomaterial, C_{60}, were generated using PEG as a carrier. The ability to pattern fullerenes is particularly important because of their potential application in nanoelectronics. Feature sizes as small as 80 nm could be easily obtained at a contact time of 4 s. Using contact times of 64, 32, and 16 s, features of 21.8, 14.6 and 9.8 nm in height were produced (Table 1), respectively.

As proof-of-concept and to confirm that C_{60} molecules are indeed patterned inside these DPN-generated features, a fullerene-based field-effect transistor was built by DPN. Lines of fullerene/PEO ink were generated across a nanoelectrode with a gap size of 500 nm that was fabricated by electron-beam lithography. The AFM image in Figure 5E shows two crossed, continuous lines wired across these gaps. Current-voltage (I-V) measurements of the output current of this device at voltages ranging from – 0.7 V to 0.85 V are shown in Figure 5F. The black line is the I-V response of the transistor measured in a dark environment, while the red line shows the current obtained under illumination with a Xe lamp (150 W). This increase in current (~ 6 times more, ~ 0.015 pA at 0.85 V vs. ~ 0.10 pA at 0.85 V) is the characteristic response of the C_{60} molecules to light illumination and proves that the photoactive C60 molecules exist in an active state inside the DPN-generated patterns. In addition, the precise delivery of C_{60}/PEO lines in the 500 nm gapped nanoelectrode demonstrates the high spatial registration of DPN.

Agarose-assisted DPN

Biological microarray technology has led to significant advances in biology, biochemistry, and medicine. These arrays form the cornerstone of modern genomics and proteomics, with many applications in gene profiling, protein screening, and drug discovery. In their current formats, spot diameters typically range from 1 to 150 μm. Recent studies have focused on decreasing feature size because high density biomolecule arrays allow one to extract more information per unit area, increase sensitivity, and use smaller sample volumes. In addition, with nanoscale features, one can essentially place an entire array underneath a single cell and probe both monovalent and multivalent cell−surface interactions. Also, with nanoscale features, one can manipulate individual biological constructs such as viruses and perhaps even proteins at the single particle level. In all of these applications, facile signal quantification requires homogeneity in both feature size and the density of biomolecules within an array. Consequently,

it is necessary to achieve this feature size reduction while maintaining the ability to create homogeneous spots for each biomolecule within and between arrays.

A variety of methods have been used to deposit DNA and proteins on surfaces with nanoscale resolution. These include several types of scanning probe lithography, e-beam lithography, nanocontact printing, and nanoimprint lithography. One tool that is particularly attractive in this regard is the scanning probe technique known as DPN. DPN has sub-50 nm resolution, is soft matter-compatible, and has the registration requirements to make high quality arrays of biological molecules. In addition, in combination with both 1-dimensional (1-D) and 2-dimensional (2-D) cantilever arrays and the related scanning probe contact printing technique, PPL, DPN has recently been transformed from a serial into a massively parallel method, with as many as 11 million pens drawing nanostructures at a rate of 7 trillion features per minute.

There are several challenges associated with using direct-write scanning probe techniques such as DPN in the large-scale parallel generation of biological arrays. The first involves transport, and specifically, ways to facilitate the movement of large macromolecules from the surface of an AFM tip to the substrate one intends to pattern. To solve this problem, many strategies have been attempted with varying degrees of success. These include tip modification procedures that change the adhesion properties of the tip for biomolecules, the use of specialty substrates such as Ni with His-tagged ink moieties, and nanopipettes with ink-transport facilitated by capillary action. Indirect patterning methods have been explored to circumvent the issue of directly transporting high molecular weight species. However, direct write techniques are preferable, resulting in decreased cross contamination between biological entities during multiplexed deposition.

The second challenge pertains to the differences in diffusion properties for different molecules. With one molecule type, tip-substrate contact-time and humidity are typically used to control transport rates. These parameters are very effective in the context of generating single ink structures. However, with a combinatorial library of biomolecules, each ink will have a different set of diffusion and adhesion properties. Therefore, the challenge of simultaneously transporting many different molecules with control over feature size is daunting in the context of a conventional DPN experiment.

The third challenge pertains to bioactivity. One must develop ways of transporting the desired molecules in such a way that they maintain their biorecognition properties. A single, general method for patterning different types of biomolecules that enables direct transport to the surface while preserving their biological activity would be highly desirable for large scale parallel generation of biomolecule arrays.

Herein, we describe the use of agarose as a universal carrier matrix to deposit proteins and DNA, the two most important classes of biomolecules, on a substrate with nanoscale resolution. The transfer of a matrix along with the analyte during DPN patterning has been observed by our group. Nevertheless, to the best of our knowledge this is the first report where the composition of the matrix may be systematically adjusted to control deposition.

Agarose is a linear biocompatible polysaccharide, composed of alternating (1−3)-linked β-*D*-galactose and (1−4)-linked (3−6)-anhydro-α-*L*-galactose that becomes a thermo-reversible hydrogel when heated in water. It has been used extensively in biology as a stabilizer andsupport for many types of biomolecules and may be fashioned into a stamp for contact printing.

In the work described herein, however, the agarose gel is not only used as a stabilizer but also as a carrier, where it is transferred as a matrix with the desired biomolecule to a substrate in the conext of a DPN experiment. The use of agarose as a carrier ink has several advantages over

the direct deposition of a pure biomolecule sample for use in a DPN experiment. First, the hydrogel stabilizes and protects proteins from drying and denaturing while on the tip. Second, the increased viscosity compared to a buffered solution and the partially hydrophobic nature of the fluid gel facilitates ink adsorption on the AFM tip without prior surface modification, a requirement of several previous protocols for effecting protein adsorption and subsequent transport. Third, the fluidity of the gel may be systematically varied by controlling the concentration of agarose in addition to chemical additives (e.g., tricine buffer), providing a third parameter effecting deposition rates besides the traditional tip-substrate contact-time and humidity used in DPN.

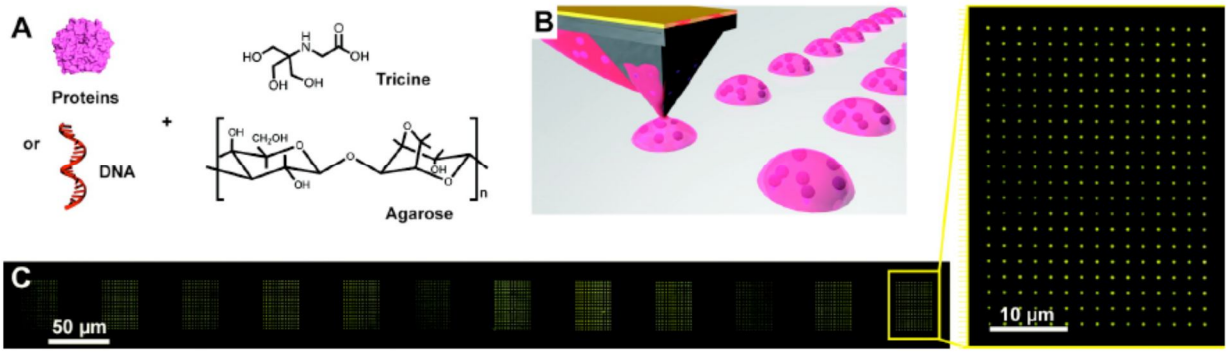

Figure 6. *(a) A schematic representation of ink and matrix components; (b) an illustration showing the process of agarose-assisted DPN; (c) epifluorescent microscope image of a 15 × 20 array of 500 nm Cy3 labeled oligonucleotide features generated in parallel from a 12-tip cantilever array.*

Our strategy for agarose-assisted DPN begins first with the preparation of an aqueous matrix composed of 0.15% agarose and an "accelerator" species containing hydroxyl, amine, or carboxylic acid functional groups used to control gel fluidity. After briefly heating until the agarose completely dissolves, proteins (0.5 mg/mL final concentration) or DNA (50 µM final concentration) is added (Fig. 6). Control over deposition parameters was examined for two model proteins, cholera toxin β subunit (CTβ) labeled with Alexa Fluor 594 and a fluorescein-labeled rabbit anti-goat IgG antibody and a 3′ heptyl amine modified oligonucleotide possessing a 5′ Cy3 label. Codelink N-hydroxysuccinimide-ester activated substrates were used to covalently immobilize the amine-modified oligonucleotides and proteins (through their exterior amine groups) by the formation of amide linkages. Significantly, the agarose matrix may be washed away, leaving only biomolecules covalently bonded to the substrate. A schematic representation of the DPN process is shown in Figure 6. By control over humidity, tip-substrate contact time, and gel fluidity, spots of either DNA or proteins are patterned in parallel with nanoscale resolution (Fig. 6C).

All DPN experiments were performed within a feedback controlled humidity chamber, which allowed for control of relative humidity between 10 to 95%. Without addition of an accelerator such as tricine to the agarose matrix, agarose transport with or without DNA or proteins did not occur on hydrophilic Codelink substrates up to 90% relative humidity. Above 90% relative humidity, agarose patterns could be imaged by AFM, though patterning was not reproducible, spatial resolution was poor, and epifluorescence microscopy indicated no significant transfer of biomolecules. A systematic study of other typical DPN parameters such as contact-time and tip speed did not further improve patterning. Furthermore, the proteins by

themselves inked from a carboxylic acid functionalized AFM tip would not transport from the tip to substrate surface.

The addition of a molecule possessing a hydroxyl, amine, or carboxylic acid functional group capable of hydrogen bonding with the agarose matrix during ink preparation facilitated transport during agarose-assisted DPN. These classes of molecules were chosen as "accelerators" because of their known ability to interact with the agarose matrix via hydrogen bonding as well as decrease the availability of water necessary for stabilization of the gel network. This, in turn, modulates the viscoelastic properties of the gels by impeding the interstrand bundling and the transformation of agarose helices into coils. Tricine, tris (1,1,1-hydroxymethyl) aminomethane (tris), tris (1,1,1-hydroxymethyl) ethane (THME), glycerol, sucrose, and ethylenediaminetetraacetic acid (EDTA) all accelerate the deposition rates for agarose-assisted DPN. In general, when progressing from the triol THME to tris (by incorporation of an amine functional group), to tricine, (which in addition included a carboxylic acid functional group), deposition rates increased for a given accelerator concentration. Thus, THME concentrations of 250−500 mM provide similar accelerating effects as tris at the 100−300 mM range, and tricine at the 10−75 mM range. With four carboxylic acid functional groups, EDTA provided the greatest accelerating effects, performing comparably to those above at concentrations of 1−30 mM. Conversely, sodium chloride provided no ability to accelerate deposition rates up to 1 M concentration. Both tris and EDTA were discarded as potential accelerators for agaroseassisted DPN, as tris contains a primary amine, which is incompatible with amine-based immobilization strategies, whereas EDTA is known to sequester metal ions from proteins, affecting their biological activity.

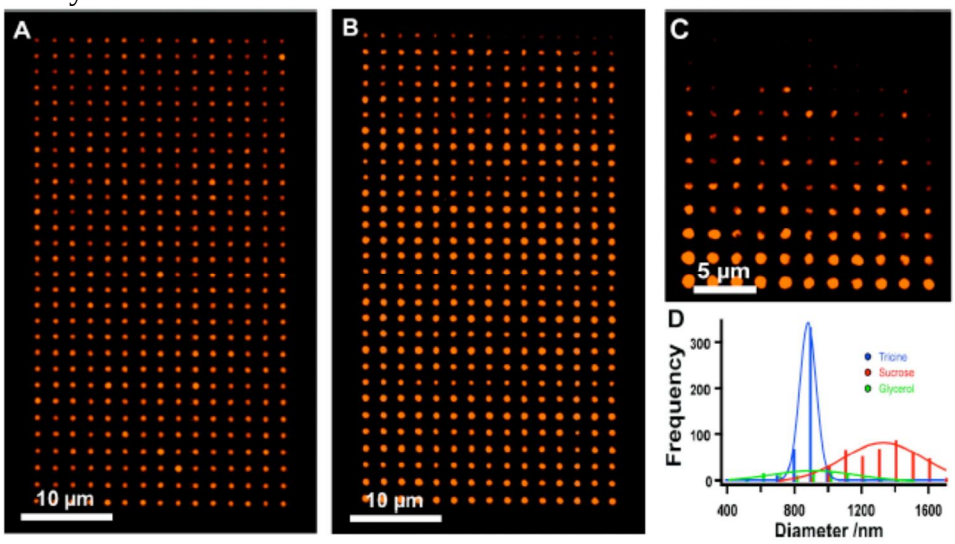

Figure 7. *Fluorescence microscope image of CTβ deposited by agarose assisted DPN using (a) tricine, (b) sucrose, and (c) glycerol as accelerating agents. In each array, features were patterned beginning with the lower left and moving right, then up to the next row and left, in a snake-like pattern. (d) Histogram of spots patterned in panels a, b, and c.*

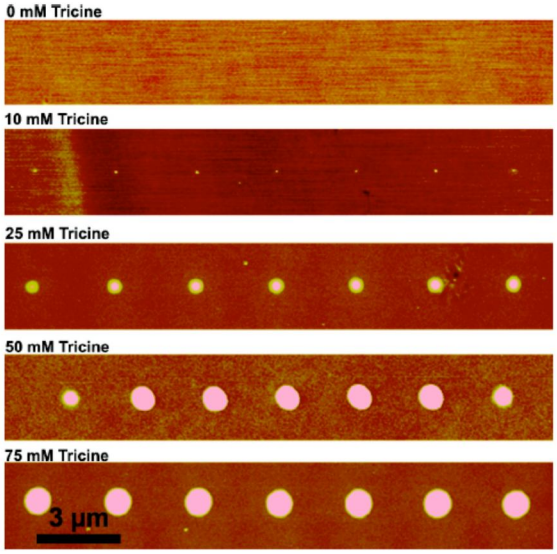

Figure 8. *Spots generated by agarose-assisted DPN with increasing tricine concentration from 0−75 mM at 0.5 s dwell time and 50% humidity.*

Tricine, sucrose, and glycerol were further examined as accelerating agents for agarose-assisted DPN according to two conditions, the ability to generate large-scale arrays and form homogeneous features within an array. Three AFM tips were coated with one of the three different agarose/accelerator matrices, also including CTβ, and used for DPN experiments at 50% humidity (Fig. 7). Arrays of 450 spots were generated for matrix inks that included tricine and sucrose, and an array of 121 spots was generated for the glycerol matrix ink. Each array was subsequently analyzed by fluorescence microscopy. Tricine provided the best results for creating large-scale arrays with homogeneous distribution. When sucrose was used as the accelerating entity, inhomogeneous feature sizes, varying in diameter by 50%, were obtained. For glycerol, the feature size decreased by ~60% over the array, with feature size progressively decreasing with each additional spot.

The feature sizes obtained from agarose assisted DPN could be controlled by adjusting tricine concentration. As a proof of concept, a series of seven dots was patterned with a 0.5 s contact time for a CTβ matrix ink with tricine concentrations ranging from 0−75 mM at 50% humidity (Fig. 8). Spot sizes increased from 0 (i.e., no deposition at 0 mM tricine) to 111 ± 10, 555 ± 32, 869 ± 83, and 962 ± 79 nm for 10, 25, 50, and 75 mM tricine, respectively. This increase in feature size occurs for two reasons. First, the tricine is partially hygroscopic, causing moisture to be extracted from the air to keep the gel hydrated thus maintaining gel fluidity compared to a matrix without tricine. Second, the additives themselves interact with the agarose matrix via hydrogen bonding, modifying the viscoelastic properties of the gel and allowing it to flow more easily from the tip to the substrate.

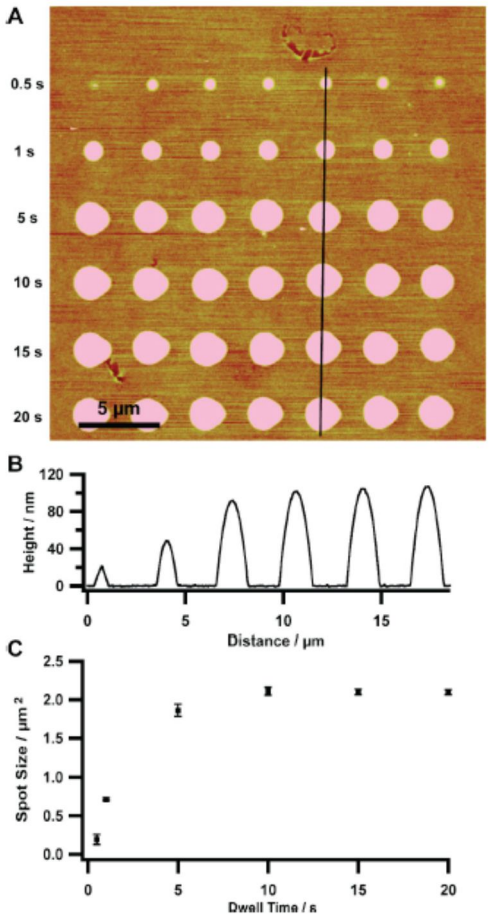

Figure 9. *A typical experiment showing saturation behavior for the deposition of anti-goat IgG by agarose-assisted DPN with a 10 mM tricine concentration. (a) Tapping mode AFM image of agarose IgG spots created with 0.5−20 s contact-time. (b) Height profile for spots from panel A. (c) Plot of dwell time vs spot size for the same experiment as in panel (a). Note that the deposition process begins to saturate both laterally and vertically after approximately 5 s dwell time.*

The deposition process was further examined by varying both tricine and tipsubstrate contact time. In a typical experiment, the contact-time between an agarose/tricine/biomolecule-coated AFM tip and substrate was varied and subsequently scanned by tapping mode AFM to determine feature size (Figure 9). For long dwell times up to 20 s, the deposition process displayed limiting behavior (Figure 9), in contrast to previous studies of alkanethiols on a gold surface. Whereas conventional DPN of alkanethiols takes advantage of a water meniscus to facilitate the transport of a dry ink to the surface, the agarose matrix is deposited as a wet gel. Further, alkanethiols chemisorb to a gold substrate, as opposed to the agarose matrix, which interacts with the surface via physisorption. This behavior of liquid spotting by DPN has been recently observed for the DPN deposition of a wet solution of Ag nanoparticles in glycerol. Similarly, the agarose ink deposition reached a point where feature size did not increase with increasing tip-substrate contact-time.

For short dwell times, generally less than 5 s, however, the deposition process may be modeled with a linear increase in spot area for increasing dwell times, predicted theoretically and

observed experimentally for materials ranging from alkanethiols and silazanes to oligonucleotides and salts. The dwell time at which the deposition process switched between linear and nonlinear behavior generally decreased for increasing tricine concentrations, although it was partly dependent on inking conditions. For a 10 mM tricine concentration, a linear deposition process was typically observed up to 5 s contact time, while linear deposition resulted for up to 1 s for 75 mM tricine concentration.

We hypothesized that the fluidity of the agarose matrix ink would be the dominant factor in determining transport rates, resulting in identical feature sizes for different biomolecules deposited by agarose-assisted DPN. To prove the same deposition rate could be obtained for two separate agarose matrix protein inks given identical tip morphology and inking conditions, a single tip was used to pattern both proteins, each inked from the same inkwell channel. Interestingly, these proteins could not be deposited by previously reported DPN procedures on Codelink substrates. The tip was first conditioned by inking with a 10 mM tricine, CTβ agarose matrix. The tip was washed in DI water for 1 min and re-inked with the same agarose matrix, and the deposition rate was examined at 60% relative humidity by varying contact-time with subsequent imaging by tapping mode AFM. The same tip was again washed in DI water for 1 min, inked with a 10 mM tricine antigoat IgG agarose ink, and again used to determine the deposition rate at 60% relative humidity (Fig. 10). Within experimental error, both protein inks exhibit nearly identical spot sizes for each dwell time and show deposition rates of 0.94 $\mu m \cdot s^{-1}$. This is a significant observation, as proteins often transport at different rates as a function of size and chemical makeup.

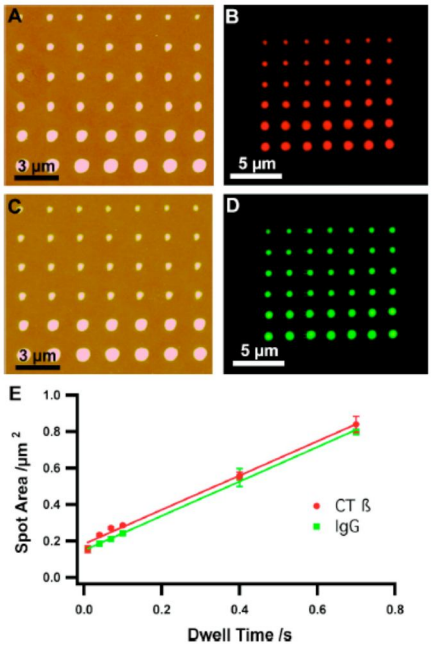

Figure 10. *Tapping mode AFM images, (a, c) and epifluorescent images (b, d) of CTβ and IgG, respectively, deposited from the same tip using agarose-assisted DPN. Note that cross contamination of IgG with CTβ during the second inking process cannot be observed by epifluorescent microscopy. (e) Plot of spot size vs dwell time for each ink as determined by the AFM images in panel (a)and (c). Given consistent tip morphology and inking conditions, agarose-assisted DPN may be used to pattern multiple proteins with the same feature sizes for the same dwell times.*

Using agarose-assisted DPN, it is possible to pattern nanoscale protein features at extremely fast rates. Typical deposition rates were on the order of 1 $\mu m^2 \cdot s^{-1}$, which is an order of magnitude greater than the fastest observed diffusion rates of MHA on gold and 1−3 orders of magnitude greater than rates previously observed for proteins or oligonucleotides. By setting a dwell time of 10 ms (the shortest time allowed by our instrument), it was possible to make an arrays of 450 features in approximately 1 min. In fact, the time to move between features took longer than the combined tip-substrate contact-time.

The biological activity and specificity as well as verification of immobilization on the functionalized surface were verified by epifluorescence microscopy for both protein and oligonucleotide arrays. A 15 × 30 dot array of Alexa Fluor 594 labeled CTβ proteins was generated by agarose-assisted DPN from 10 mM tricine agarose matrix (Figure 10). On the same substrate, a second array of antigoat IgG antibodies was patterned as a control (Fig. 11). The proteins were allowed to react with the surface for 4 h and then washed with PBS buffer to remove the matrix, leaving biomolecules covalently immobilized on the surface. Significantly, after washing, no matrix could be detected by AFM. After passivation with an amine-terminated polyethylene glycol to prevent nonspecific adsorption, the protein patterned substrate was challenged with an Alexa Fluor 488-labeled anticholera toxin antibody for 30 min at room temperature. After washing, the substrate was blown dry with N_2 and imaged by epifluorecent microscopy. Figure 10 clearly indicates antibody-antigen binding between anticholera toxin to the CTβ arrays with a signal-to-noise of 2:1, while the antigoat IgG provides a negative control with minimal cross reactivity.

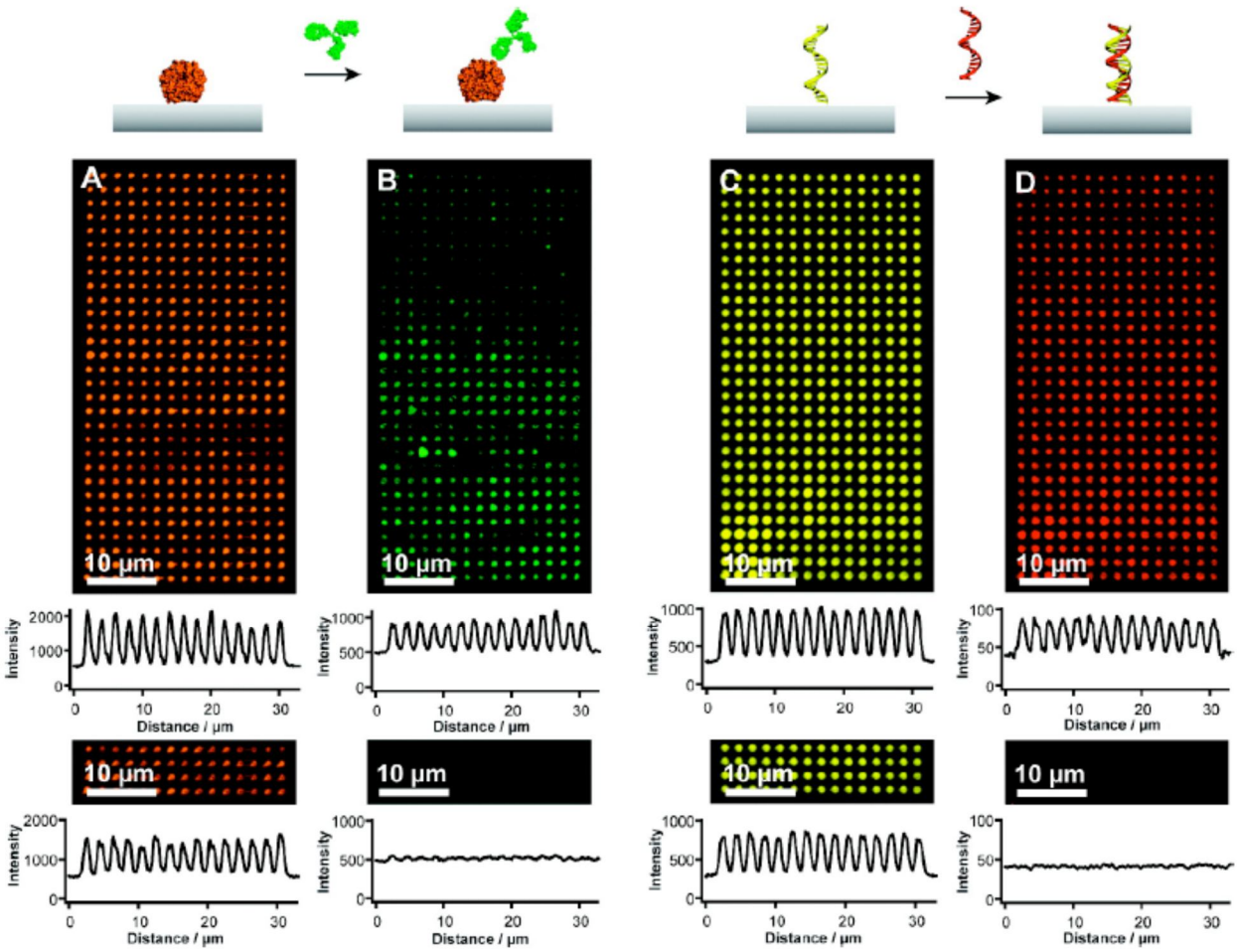

Figure 11. *Simultaneous imaging before and after protein antigen binding (a and b) and hybridization (c and d) with negative controls. Alexa Fluor 594 labeled CTβ spotted by agarose-assisted DPN (a, upper image) used for antigen binding and Alexa Fluor 594 labeled antigoat IgG (a, bottom image) used as a negative control. (b) After probing with Alexa Fluor 488-labeled anticholera toxin showing antigen binding (upper panel) and negative control (lower panel). (c) Cy3-labeled amine modified oligonucleotides with a complementary sequence (upper panel) and a Cy3 labeled amine modified random sequence (lower panel). (d) After hybridization with complementary probe showing hybridization (upper panel) and negative control (lower panel).*

Similarly, an array of Cy3-labeled oligonucleotides was generated by agarose-assisted DPN employing 10 mM tricine concentration (Figure 11). Simultaneously, a negative control random sequence was spotted at a different location on the same substrate by agarose-assisted DPN. After the oligonucleotides had reacted with the surface, the substrate was passivated with ethanolamine and subsequently immersed in a 1 µM aqueous buffered solution (60 mM trisodium citrate, 600 mM NaCl) of a Cy5-labeled probe sequence at 45°C overnight. Excess probes were removed by washing under vigorous agitation and the substrate was blown dry with N_2. Upon imaging, it is clear that the probe sequence binds its target with signal-to-noise ratios greater than 2:1 at, and only at, the locations of the complementary sequence (Figure 11). From a technical standpoint, agarose-assisted DPN allows for protein patterning at ambient humidity; it

is unnecessary to use a relative humidity upward of 80% to both affect protein deposition and maintain biological activity as was necessary in several previous studies. This results in decreased wear on the piezo elements of the AFM.

In this work we have shown agarose to be an effective matrix to control the deposition process of biomolecules by DPN. The deposition rate may be systematically varied between 0 and 1.5 $\mu m^2 \cdot s^{-1}$ by controlling the concentration of an accelerator such as tricine buffer within the matrix. This provides a third handle to control deposition in addition to the traditional tipsubstrate contact-time and humidity used in conventional DPN. Importantly, one can use the agarose and an appropriate amount of accelerator to modulate the rate of protein/matrix transport so that one can realize similar feature sizes from proteins that normally do not transport or transport at different rates in the absence of the accelerators. The agarose matrix may be easily washed away, leaving either proteins or oligonucleotides covalently bonded to the substrate. Though uniformity in terms of tip morphology, array linearity, and inking remain challenging, improvements in methodology of fabricating tip arrays combined with more uniform inking methods will allow for parallel multiplexed biomolecule deposition, each with the same spot size for facile comparison of signal intensity. Significantly, these biomolecules retain activity once attached to the surface, and extreme care need not be used to keep proteins from denaturing on the tip surface. Agarose-assisted DPN is an extremely quick patterning method with deposition rates up to 3 orders of magnitude faster than previously reported printing of biomolecules, which overall decreases time and costs for printing nanoscale biomolecule features by DPN. Utilizing massively parallel 2-D tip arrays it should be possible to print nanoscale biomolecule dots at rates of 50 million features per min with densities of 25 million spots per cm^2.

A.3. Inking Individual Tips with Specified Biomolecules

Multiplexed Pen Inking by Inkjet Printing

Over the past year a novel approach to inking pen arrays was developed that addresses the multiplexed inking challenge in the context of DPN and related nanolithographies. Specifically, pens within 1D or 2D arrays were independently addressed with chemically distinct inks using an inkjet printer and a new surfacemodification strategy was introduced that directs the ink droplet to the tips of the cantilevers. This method of delivery provides control over the inking process and transforms DPN into a general nanofabrication tool that uniquely combines high throughput, high resolution, and multiplexing capabilities (Fig. 12A).

Using a remote piezoelectric-controlled nozzle, the inkjet printer can directly deliver pico to nanoliter volumes of ink to each pen. In air, the droplet diameters range from 40 to 100 μm, but increase to several hundred micrometers upon contact with the substrate. This inking protocol allows for the delivery of a large number of chemically distinct inks to individual pens in a 1D or 2D pen array. To evaluate this approach, we initially studied the ability to address and coat every other pen in a 7-pen 1D array with an MHA/ethanol solution (10 μM, ~320 pL droplets), as shown in figure 12B. The ink coated pen array was then used in a DPN experiment to generate a 4 x 4 array of MHA features of 1.5 μm in diameter on a gold thin-film substrate. Subsequent etching of the exposed gold left raised features that could be easily characterized by optical microscopy (Fig. 12C). Note that only the four inked cantilevers produced patterns. This experiment demonstrates that cantilevers spaced 150 μm apart can be addressed without cross-contamination.

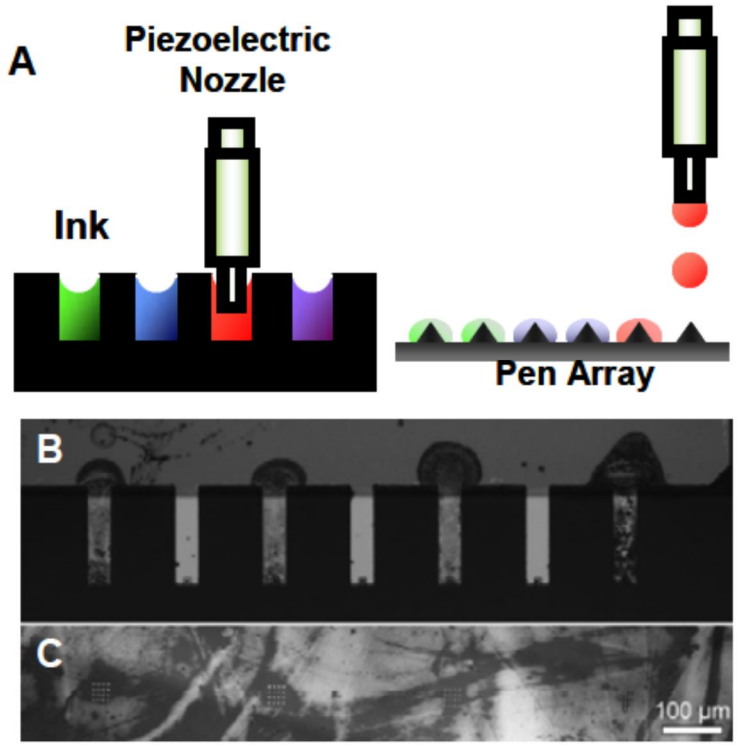

Figure 12. *(A) Scheme for addressable inking of pen arrays by inkjet printing. (B) Optical image of a 1D pen array with alternating pens inked with 1 drop of MHAethanol solution (10mM, 320 pL), and (C) the corresponding gold nanostructures patterned with the inked pen array.*

Importantly, it was found that delivering the same amount of MHA ink to different pens in an array using inkjet printing yields pattern features of similar size. Pattern sizes were measured by in situ lateral force microscopy (LFM) of the MHA patterns, by examining the aforementioned raised gold structures via optical microscopy, and also by AFM. The standard deviation of feature sizes generated by four different pens in the same array was 4.4±1.4% and increased only slightly to 4.8±0.7% among different pen arrays. This size variation is remarkably small compared to dip-coated pen arrays, whose ink diffusion rates can vary by more than 10% from pen to pen (standard deviation) and are arbitrary from array to array. The inked pen arrays have a shelf-life of at least one month and can generate high quality features down to 100 nm with less than a 10% feature size variation.

To evaluate the prospects for multiplexing, alternating cantilevers within a 7-pen array were inked with different fluorophorelabeled phospholipids, by programming a single inkjet nozzle to go through cycles of aspiration, dispensing (inking), and cleaning for each of the four inks. This pattern demonstrates that inkjet printing can enable multiplexed DPN with multiple inks.

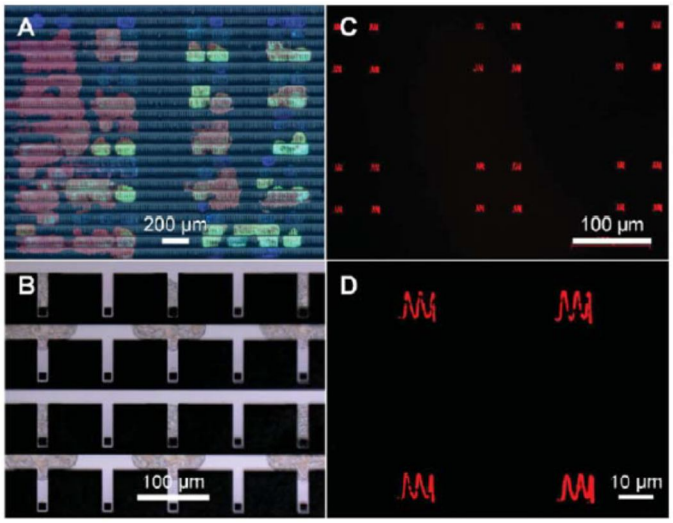

Figure 13. *Addressable inking of 2D pen arrays with phospholipids. (A) Four fluorophore labeled phospholipids printed on a 2D pen array (90mm X 20mm spacing). (B) Rhodamine labeled phospholipid addressed to every other pen in a 2D array (90mm X 90mm spacing), and (C, D) the corresponding 700 nm line width patterns written on a glass slide. Note that the cross-talk problem encountered in (A) is eliminated when the pen-to-pen spacing is increased to 90mm X 90 mm.*

Multiplexed inking of 2D arrays with multiple fluorophore-labeled phospholipids is also possible. In a proof-of-concept experiment, the goldcoated tips of a 55,000-pen 2D array were functionalized with 1- mercaptoundecanol, and the remaining areas (silicon nitride and silicon/SiO2) passivated with 1-octadecyltrichlorosilane (OTS). This chemical modification step is important as it overcomes the capillary action driven adhesion of inked cantilevers to the silicon/SiO2 support. In one experiment, fluorophore-labeled phospholipids were printed on one quadrant of a 55000-pen 2D array in the pattern of ‘‘NU’’ (Fig. 13A). The inked pen array was subsequently used for DPN patterning. As a result of the 20 mm spacing between the adjacent pens of this 2D array, each inkjet droplet covered five to seven pens rather than one. Moreover, the inking was not perfectly uniform because of the spreading of the droplets once they hit the substrate. Both of these issues can be addressed by increasing the pen-to-pen spacing in the array. Indeed, as proof of concept, single-pen addressability can be achieved by using a 2D pen array with a pen-to-pen spacing of 90 µm x 90 µm (Fig. 13B–D).

Multiplexed DPN of Proteins with Inkwells

This section describes the use of 1D AFM tip arrays (Model No.: A-26, NanoInk Inc., Skokie, IL) for simultaneous multiple ink patterning via DPN. Two composite inks containing fluorophore labeled BSA (green) and anti-ubiquitin (red), were coated onto alternating AFM probes using inkwells (NanoInk Inc., Skokie, IL) specially designed for such tip-inking. Both the optical microscopy images of the inkwell and the AFM tip arrays before and after ink-coating are shown in figure 14. The diffusion rates of the two inks have been shown previously to be very similar for the ratio of 1:5 for both BSA:PEG and anti-ubiquitin:PEG. The fluorescent images (Figs. 14E, F) clearly show that the two different biomolecules (BSA in green and antiubiquitin in red) are simultaneously patterned into the designed array format, and the zoomed-in image shows the fluorescent signal with more details and clearer contrast. In order to compare the

variation of the generated pattern sizes and to characterize the generated dot sizes, AFM images of the DPN features were taken. At a tip-substrate contact time of 32 sec, the average dot diameter is 328 nm for BSA and 306 nm for antiubiquitin, which is less than 7% variation. Significantly, if not mixed with PEG, the generated dot sizes would be 284 nm and 223 nm, respectively.

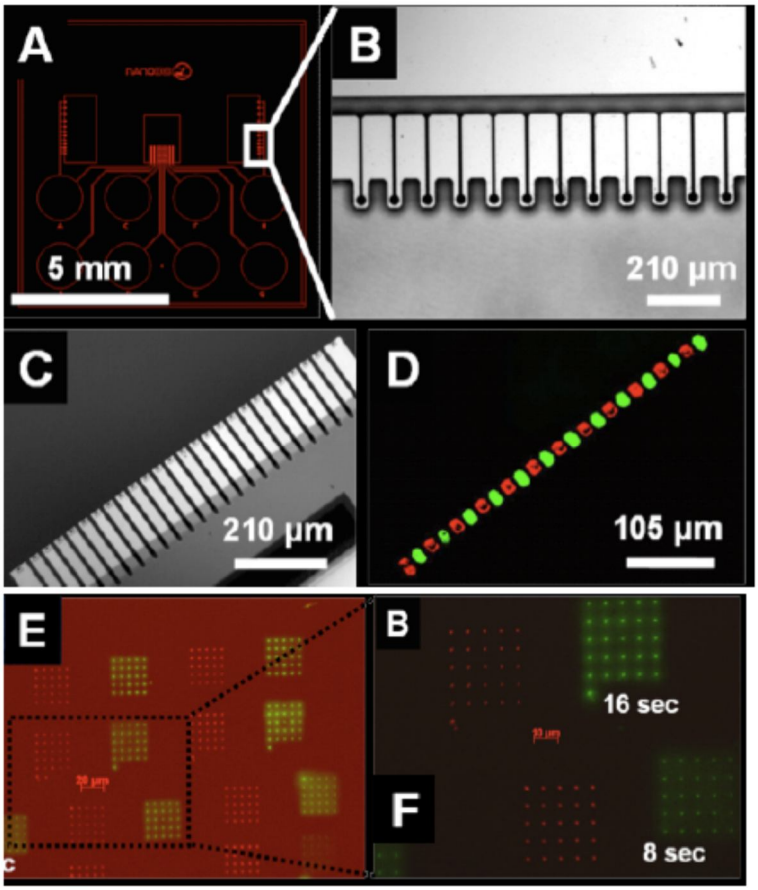

Figure 14. *(A) Overview and (B) zoom-in of the inkwell used for coating of alternating AFM tips with BSA/PEG and anti-ubiquitin/PEG). Optical (C) and (D) fluorescent microscopy images of the AFM tip array (A-26) used for DPN patterning with multiple inks. The AFM tips were coated with BSA/PEG (green) and anti-ubiquitin/PEG (red), both at a ratio of 1:5. (E) Fluorescent image of DPN generated dot arrays. (F) Zoomed-in image of the area within the rectangle in (E), showing*

Multiplexed DPN of Lipids by Inkwell Inking

Perhaps the most unique capability of multiplexed DPN is its ability to integrate different ink materials into complex, combinatorial structural and compositional libraries at high (e.g., subcellular) lateral resolution. To demonstrate this capability, a single cantilever array was used to simultaneously pattern arrays of features composed of DOPC doped with 1 mol% of rhodamine-labeled and fluorescein-labeled lipids. Microfluidic inkwells capable of simultaneously delivering different lipid mixtures to eight different tips in a 26-tip array were used to address the tips (Fig. 15). It was previously observed that the multilayers are fluid at high humidity (>40%). When distinct pattern compartments are connected (top row, Fig. 15C), the patterns are contiguous and retain their lateral fluidity. Control patterns that are not connected

(bottom row, Fig. 15C) confirm that the mixing takes place on the patterned surface. Since the red/green ratios in the fluorescence signal of the nanostructures correspond to the amount of ink in each patterned reservoir, this method of mixing lipids on the canvas opens the possibility to create different combinations on the surface from a limited number of inks on the tips.

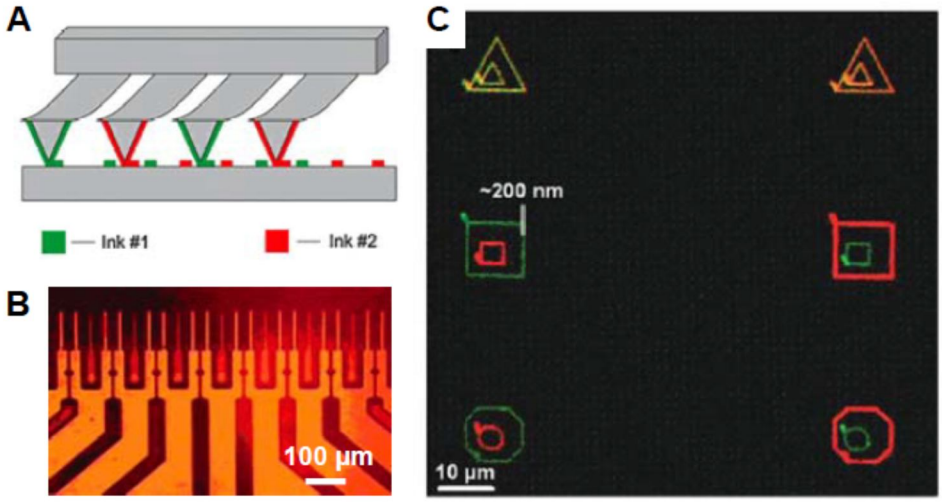

Figure 15. *Multiplexed lipid integration for combinatorial nanostructure libraries. (A) Schematic illustration of a method to pattern different lipids on subcellular scales using a single multiplexing DPN cantilever array. (B) Optical image of an inkwell used for inking. (C) Multichannel fluorescence images of multilayer structures composed of DOPC doped with two different fluorophore-labeled lipids (rhodamine/red and fluorescein/green) integrated with bulls eyes of different shape and topology on subcellular scales. The top two triangle patterns were connected and the two inks mixed to form yellow and orange patterns (depending on the ratios of the red and green pattern volumes), indicating the fluidity of the patterns as well as the possibility of mixing lipids in different amounts using only two different starting inks.*

A Self-Correcting Inking Strategy by Chemical Modification of AFM tips

Despite the addressability afforded by inkjet printing, the spatial resolution of inking is constrained by mechanical hysteresis, which limits registration of the inkjet printer with the pens in the array, and as a result, the ability of an inkjet printer to independently ink tips in an array. To overcome these problems, a self-correcting inking strategy was developed that allows directed drying of the ink droplet based on chemical wetting and surface modification protocols (Fig. 16). The basic idea is to functionalize the pens anisotropically so that the pyramidal tip is hydrophilic and the remaining area is hydrophobic. The anisotropic functionalization facilitates localization of an ink droplet on the hydrophilic tip as a result of differences in surface energy. As proof of concept, the tips of an array were selectively coated with a thin layer of gold using a cover slip as a shadow mask. This approach allows one to locally functionalize the tip area with MHA through alkanethiol - gold chemistry (Fig. 17). Because the gold deposition step can be integrated into the mold-and-transfer pen microfabrication process, this anisotropic functionalization strategy can be conveniently applied to both individual AFM cantilevers and pen arrays. Using this approach and an inkjet printer to deliver 320 pL droplets onto individual pens within the array, such structures could be selectively addressed without contaminating neighboring pens (Fig. 17A). The ink droplet was localized within the MHA functionalized tip area, an area which is less than 2% of the total footprint area for an MHA/ethanol droplet drying on a MHA functionalized gold substrate. This experiment, however, does not demonstrate the

selective ink localization from the cantilever arm to the tip. To evaluate localization, a 0.2 µL droplet of 2 µM MHA/ethanol solution was deposited on the cantilever and tip areas of a 7-pen array (Fig. 17B, five pens shown). Optical microscopy showed that as the droplet dries, the ink moves from the hydrophobic cantilever arm to the hydrophilic tip. The liquid film breaks up at the hydrophobic-hydrophilic boundary, thereby confining the ink to the tip area (Fig. 17B). A control experiment shows that the ink dries randomly on native Si_xN_y cantilevers.

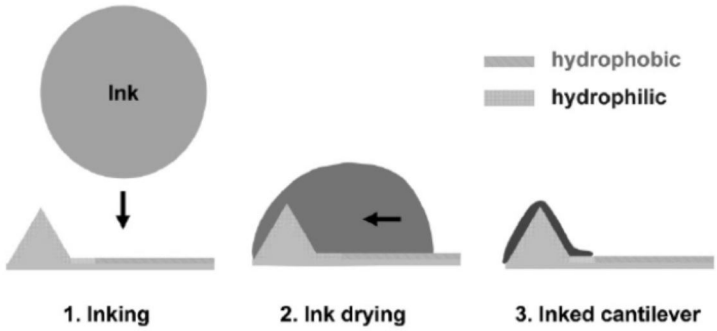

Figure 16. *Self-correcting inking of an anisotropically functionalized pen. The pen is functionalized such that the tip area is hydrophilic (MHA functionalization) and the remaining areas hydrophobic (ODT functionalization). Ink molecules are preferentially driven to the hydrophilic area due to differences in surface energy.*

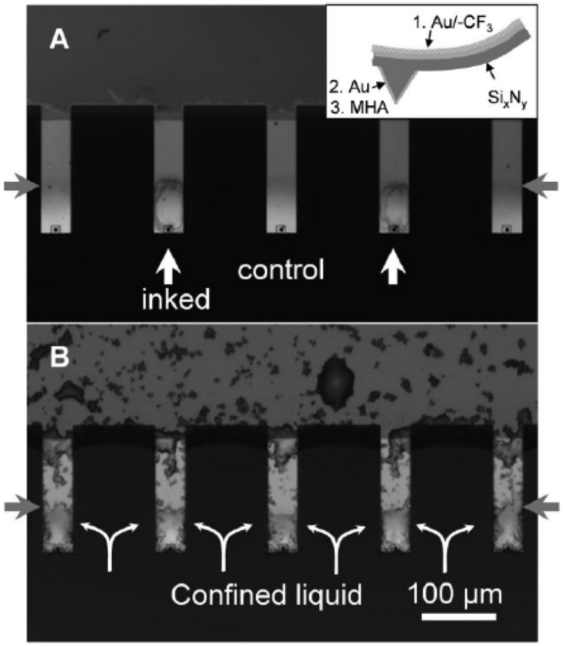

Figure 17. *Self-correcting inking of anisotropically functionalized pens. (A) Addressable inking of pens (white arrows) in a pen array by inkjet printing of 3 drops of a 10mM MHA/ethanol solution (320 pL each) on each tip. The anisotropically functionalized areas (boundary marked by grey arrows) dictate where the ink droplet dried. The inset shows anisotropic functionalization of the AFM probes. (B) Optical microscopy image of anisotropically functionalized pens dip-coated in an MHA/ethanol solution. Note that the ink is confined to the hydrophilic tip areas.*

Taken together, the inkjet and self-correcting inking strategy reported here provide a versatile and high-resolution method of addressing the multiplexed-inking challenge for DPN with 1D and 2D cantilever arrays. This work marks an important step towards the realization and practice of high throughput, multiplexed, and consistent nanoscale patterning of soft matter. Considering the versatility of DPN for many types of inks, it should be possible to extend this strategy to many classes of important molecules, including DNA, peptides, proteins, and other vchemically and biologically relevant materials.

Polymer Pen Lithography (PPL)

For multiplexed patterning synthesis of materials over large areas with high throughput and low cost, a massively parallel lithographic method is needed. Due to its serial nature, single pen DPN has limited throughput capabilities. Recently researchers have demonstrated the fabrication of patterned structures of molecule-based materials using 2D cantilever arrays with up to 1 million pens over areas as large as square centimeters. However, these arrays are fragile and quite costly. Indeed, no simple strategy exists that allows one to rapidly pattern molecule based features with sizes ranging from the nano- to millimeter scale in a parallel, high throughput, and direct-write manner. In recent years, a simple cantilever-free lithographic approach called polymer pen lithography (PPL) was developed in our lab (Figs. 18, 19). PPL allows arbitrary patterns to be printed with feature sizes ranging from 90 nm to 100 μm simply by changing the force and tip-substrate contact time over which the ink is delivered.

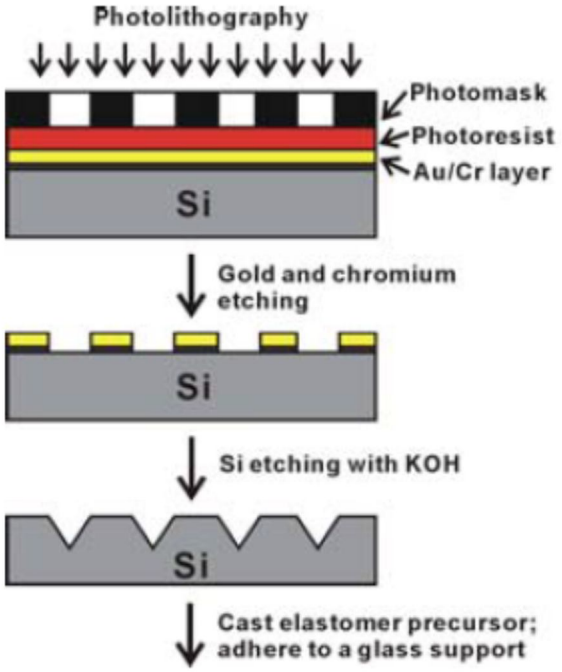

Figure 18. *Schematic diagram of the polymer pen array fabrication process.*

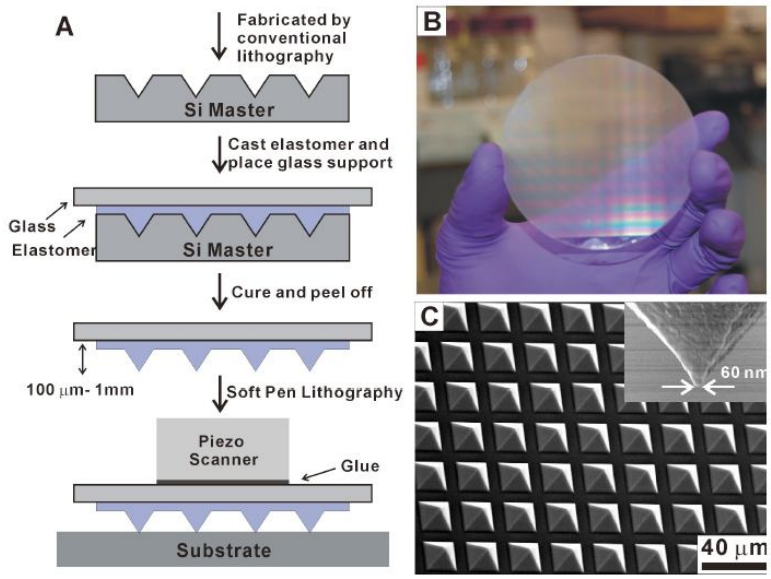

Figure 19. *A) A schematic illustration of the PPL setup. B) A photograph of a 10 million pen array. C) SEM image of the soft pen array. The average size of the tip radius of curvature is 70 ± 10 nm (inset).*

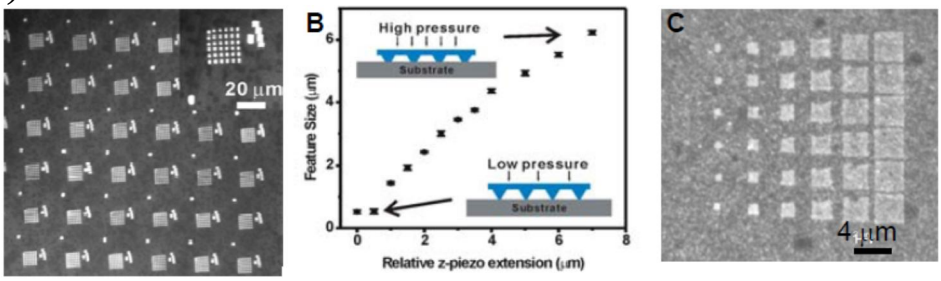

Figure 20. *(A) Optical image of a 480 mm × 360 mm section of an one million gold dot array (6×6 within each block) on a silicon substrate (using a pen array with 28,000 pyramid-shaped tips). (B) MHA dot size as a function of relative z-piezo extension. The results were obtained using a polymer pen array with 15,000 pyramid-shaped tips at 25 oC and a relative humidity of 40%. (C) Optical image of arrays of gold squares generated at different z-piezo extensions using a pen array with 28,000 pyramid-shaped tips.*

A defining characteristic of PPL, compared to DPN and most contact printing strategies, is that PPL exhibits both time- and force-dependent ink transport. As with DPN, the size of PPL features is linearly dependent on the square root of the tip-substrate contact time. This property of PPL, which is a result of the diffusive characteristics of the ink and the small size of the delivery tips, allowed us to pattern submicrometer features with high precision and reproducibility (variation of feature size is less than 10% under the same experimental conditions). The force dependence of PPL derives from the "soft" nature of the elastomer pyramid array. Indeed, the microscopic pyramidal tips can be made to deform with increasing amounts of applied force, which can be controlled by simply extending the z-piezo in the vertical direction. Although such a deformation has been regarded as a major drawback in contact printing (it can result in "roof" collapse and limit feature size resolution), with PPL, the controlled tip deformation can be used as an adjustable variable, allowing control of the tip substrate contact area and the resulting feature size. Within the force range allowed by z-piezo

extension, a linear relationship between piezo extension and feature size at a fixed contact time of 1 s was observed (Fig. 20).

Because of the dependence of the feature size on the applied force, large features were generated by controlled piezo extension rather than the more time consuming meniscus formation and ink spreading. Indeed, nano- or micrometer sized features can be generated in a single printing cycle by simply adjusting the degree of tip deformation. As proof-of-concept, 6×6 gold square arrays, where each square in a row was written in one printing cycle at different tip-substrate forces but a constant 1 s tip-substrate contact time, were fabricated by PPL and subsequent wet chemical etching (Figure 20). The largest and smallest gold squares are 4 μm and 600 nm on edge, respectively. Note that this experiment does not define the feature size range attainable in a PPL experiment, but rather, is a demonstration of the multiple scales accessible by PPL at a fixed tip-substrate contact time.

Unlike conventional contact printing, PPL patterns molecules with precise control over feature size, spacing, and shape. To demonstrate these capabilities, a polymer pen array of 100 pyramidal tips spaced 1 mm apart was used to generate 100 duplicates of an integrated gold circuit. The width of each electrode in the center of the circuit is 500 nm, while the width of each electrode lead going to the nanometer scale electrodes is 10 μm, and the size of the external bonding pad is 100 × 100 μm^2 (Fig. 21). To accommodate both the resolution and throughput concerns, different relative z-piezo extensions at different positions of the circuit were used, with 0, 2, and 6 μm for the central electrodes, electrode leads, and bonding pads, respectively. As a result, writing a 100×100 μm^2 area only requires 400 printing cycles (less than 0.5 s for each cycle), and the total time required to generate 100 duplicates of the circuit takes approximately 2 hr, whereas electron-beam lithography would take many days to produce a pattern on the same scale. Re-inking of the pen array is not necessary because the PDMS behaves as a reservoir for the ink throughout the experiment.

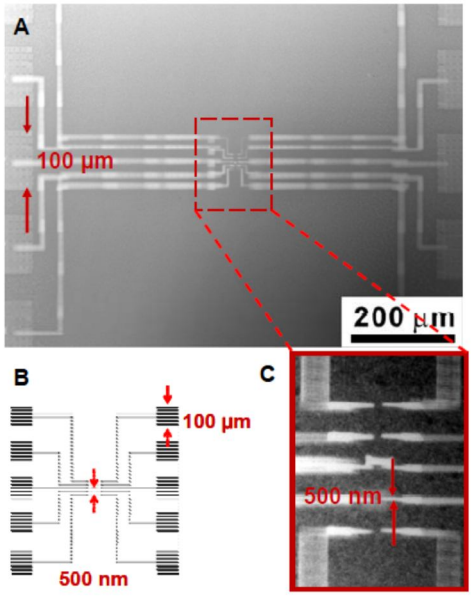

Figure 21. *(A) Optical microscope image of a multi-length scale gold circuit fabricated by PPL. (B) The bitmap design of the circuit. (C) An inset showing a magnified image of the circuit center.*

The mask-less nature of PPL allows many structural variants to be created without designing a new master via a throughput-impeded serial process. In addition, PPL can be used with sub-100 nm resolution with the registration capabilities of a closed-loop scanner. For example, PPL was used to generate 15,000 replicas of the 2008 Beijing Olympic logo on gold using MHA as ink and subsequent wet chemical etching (Fig. 22). Each logo was generated using PPL from a 70×60 μm^2 bitmap. The letters and numbers, "Beijing 2008", were generated from ~20,000 dots that were 90 nm in diameter, while the picture and Olympic rings were made from ~4,000 dots of 600 nm in diameter at higher array-substrate contact forces. These structures were created by holding the pen array at each spot for 0.05 s and traveling between spots at a speed of 60 μm/s. A representative portion of the approximately 15,000 replicas (yield > 99 %) generated across the 1 cm^2 substrate demonstrates their uniformity (Fig. 22). Importantly, the total time required to fabricate all of these structures was less than 40 min.

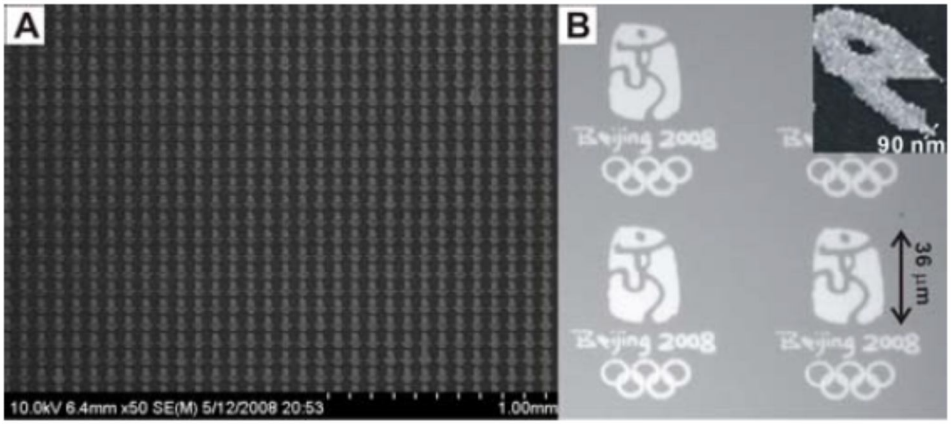

Figure 22. *(A) SEM image of a representative region of approximately 15,000 miniaturized duplicates of the 2008 Beijing Olympic logo. (B) A zoom-in optical image of a representative replica. The inset shows a magnified SEM image of the letter "e".*

The time- and force-dependent ink transport properties of the polymer pen pyramid arrays provide tunability that may allow other patterning capabilities to be developed. Because PPL is a direct-write technique, it is also ideal for fabricating arrays of structures made of soft matter, such as proteins, thus making this patterning method potentially useful in the life sciences as well.

Multiplexed Patterning with PPL

The ability to fabricate biomolecular (e.g. DNA, proteins) micro- and nano-arrays in a low cost and high throughput manner is important for a wide variety of applications, including drug screening, materials assembly, biowarfare agent detection, biosensors, and fundamental biological studies. Traditional approaches to making protein microarrays include photolithography and inkjet printing. Recently, studies also have focused on the miniaturization of biomolecule patterns into the nanometer regime because high density DNA arrays can provide increased detection sensitivity and, in principle, allow one to screen millions of disease markers with one chip. Furthermore, protein nanopatterns also can provide insight into important fundamental biological processes, such as cell adhesion and differentiation. In the past year, we have developed and studied a novel and rapid strategy for inking nanoscale probes with different

proteins, which can be transferred to a surface via the technique known as PPL. Using this approach, we have generated sub-100 nm structures at a rate of 150,000 features per second.

Many new techniques have been explored for miniaturizing protein array features, including microcontact printing, nanoimprint lithography, and a variety of scanning probe lithographies, such as dip-pen nanolithography (DPN). DPN and PPL are particularly versatile "direct write" methods which allow one to generate protein structures over large areas with submicrometer resolution using as many as 11 million pens in parallel. This approach was extended to PPL in the context of single ink structures. Importantly, the "direct write" nature of DPN and PPL minimizes ink cross contamination. By combining the advantages of inkwell inking and inkjet printing with DPN, we have demonstrated multiplexed patterning of small molecules.

Patterning multiple proteins by DPN over large areas remains a significant challenge for several reasons. (1) The opacity of Si and Si3N4 cantilevers makes it difficult, if not impossible, to align a 2D cantilever array for inking multiple proteins using inkwells. (2) The diffusion rates for different proteins can vary dramatically because of the differences in their molecular weights and structures. Such variation leads to nonuniform feature sizes for structures made with different proteins even though the tip-substrate contact time is held constant. (3) Furthermore, because the diffusion rates of proteins are typically low, the fabrication of sub-micron or micron scale protein patterns useful for optical detection purposes is a time-consuming process. (4) The 2D Si3N4 cantilever array required for large scale parallel DPN experiments is relatively costly and fragile.

In principle, PPL is particularly well-suited for patterning biomolecule structures in a multiplexed manner. Instead of relying on hard Si3N4 cantilevers, PPL utilizes a soft polymer pen array to deliver inks onto a surface by controlling the movement of the pen array with a scanning probe microscope. Unlike DPN and conventional contact printing, the feature size in a PPL experiment not only depends upon probe-substrate contact time, but also contact force (which results in the reversible flattening of the tip). In addition, the same mold used to make the array can be used as a series of inkwells that can be addressed and filled via inkjet printing. In this way, one can achieve perfect registry between the pens in the array and the inkwells. Herein, we demonstrate that one can use PPL to pattern multiplexed protein arrays in one writing step with control over feature size (spanning the sub-100 nm to many μm length scale).

In a typical experiment, the pyramid-shaped wells in a Si mould used to make a PPL array were first filled with protein inks by inkjet printing (Fig. 23A). The ink solution was composed of 0.1 to 0.5 mg/mL of protein molecules and 5 wt% of glycerol in phosphate buffered saline (PBS, pH 8.0). Note that the glycerol molecules serve as a carrier matrix to increase the mobility of the ink on the polymer pens. A Piezorray (PerkinElmer, Waltham, MA) inkjet printer was programmed through priming, aspiration, and dispense cycles to selectively address and ink each well with one 320 pL droplet of the protein ink without contaminating neighboring wells. Subsequently, a polymer pen array was treated with oxygen plasma for 30 s to render the surface hydrophilic, which minimizes the nonspecific adhesion of protein molecules. The hydrophilic pen array was placed in an NScriptor (NanoInk, Skokie, IL) nanolithography instrument and dipped in the wells by bringing the pen array into contact with the wells. We then used the inked polymer pen array to write directly on a Codelink slide, which has a surface terminated with N-hydroxysuccinimide (NHS) ester functional groups. The patterned slide was incubated overnight at 4 ºC to allow the amine groups on the proteins to react with the NHS esters. Finally, the slide was passivated with bovine serum albumin (BSA) for 1 hr, rinsed with PBS buffer, and dried.

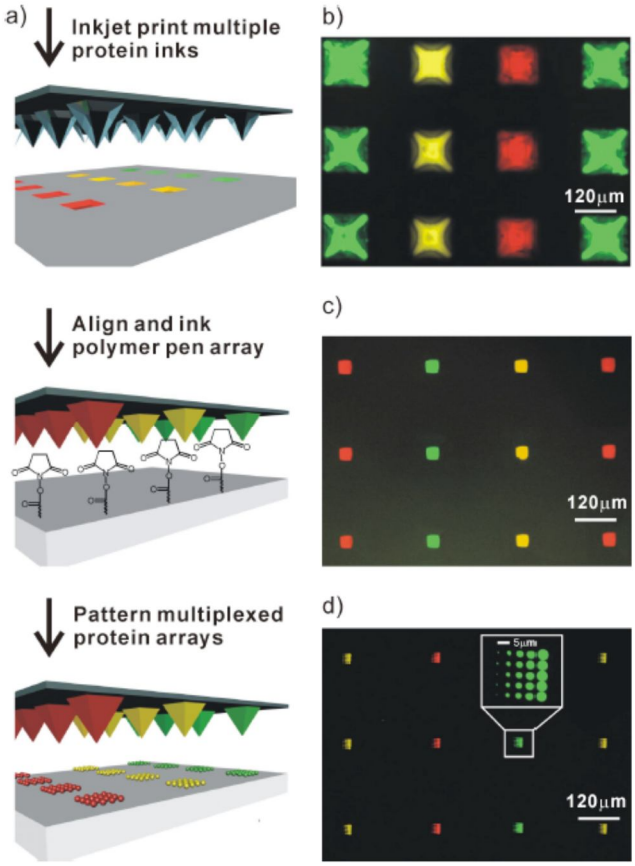

Figure 23. *(A) Schematic illustration of the PPL patterning process used for making multiplexed protein arrays. Fluorescent images of: B) a Si mould inked with 3 proteins by inkjet printing; C) a polymer pen array dipped into the Si mould in (B); D) multiplexed proteins arrays made by PPL with the polymer pen array in (C). Yellow: TRITC conjugated anti-mouse IgG; Green: Alexa Fluor 488 conjugated anti-prostate specific antigen (anti-PSA); Red: Alexa Fluor 647 conjugated anti-cholera toxin beta (anti-CTb).*

The wells in the mould are inverted pyramids with an average depth of 86 μm, edge length of 120 μm, and centre-to-centre distance of 240 μm. As a proof-of-concept, we loaded 1600 inkwells with three different dye-labeled proteins, and by fluorescence microscopy one can see that they have been properly addressed with the inkjet printer (Fig. 23B). We found that optimum results were obtained with molds pre-modified with 1H,1H,2H,2H-perfluorodecyltrichlorosilane to make the surfaces hydrophobic. By making the surface hydrophobic, the ink is driven by gravity into the wells. At present, ink wells must be separated by at least 120 μm to be compatible with the resolution of the inkjet printer (~100 μm). This limitation can be overcome with a higher resolution inkjet printer. A PPL array was then leveled, aligned, and brought into contact with the ink-filled mould by the optical microscope of the NScriptor. Importantly, because the polymer pen array is transparent, one can easily level, align, and dip this 2D pen array in the wells and confirm inking optically. The PPL array was allowed to absorb ink for 10 min at 90% relative humidity, imaged by fluorescence microscopy (Fig. 23C), and then used for patterning experiments. As a proof-of concept, each pen in an array was used to make a 5 × 5 protein dot array with 5 μm spacing between the dots (Fig. 23D). As shown in the inset image, the sizes of the protein features from left column to right column are

0.63±0.063, 1.94±0.018, 3.09±0.14, 3.94±0.093, 4.83±0.081 µm, respectively. There is no apparent cross-contamination, a consequence of the one-step, top-down writing attribute of PPL. Finally, the inkwells can be used repeatedly to ink more than five pen arrays with very similar results and less than 10% variation in feature size across the studied length scale.

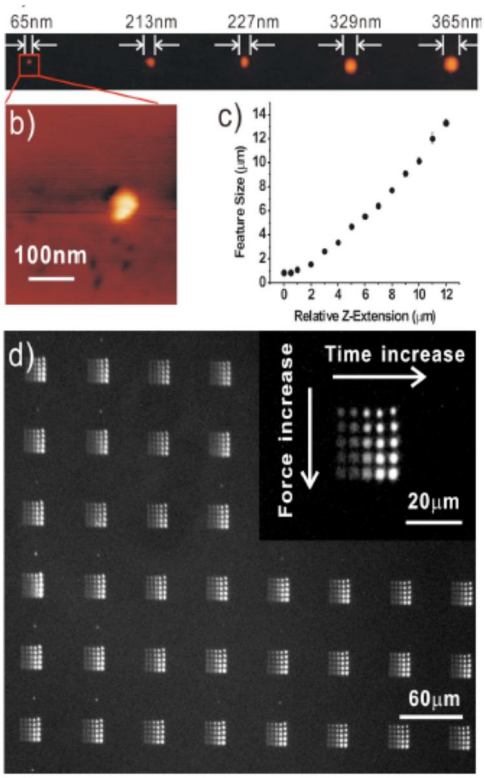

Figure 24. *A) Tapping mode atomic force microscopy (AFM, topographic mode) of CTb/glycerol patterned on a Codelink slide by PPL. B) A zoom in AFM topography of (A). C) Feature size of patterned protein arrays as a function of tip-substrate contact force. D) Fluorescent image of PSA arrays labelled with Alexa Fluor 488 conjugated anti-PSA at different tip-substrate contact time and contact force. The inset is a magnified fluorescence image.*

Importantly, one can control feature size over the sub-100 nm to many µm length scale by varying both the tip-substrate contact time and contact force (Fig. 24). When the tip makes initial contact with the substrate, 65 nm features are made at 0.01 s contact time (Figs. 24A, B). One sees the feature area dependence upon the tip-substrate contact time typical of DPN and PPL. Because feature size in a PPL experiment is also dependent upon contact force, one can rapidly access larger feature sizes by controlling Z-piezo extension (Fig. 24C). For example, with a 500 nm extension (relative to initial contact) and a fixed contact time of 10 s, the resulting protein feature size is 857 ± 40 nm. Further extending the Z-piezo results in a quasi-linear increase in feature size. For example, 13.32 ± 0.32 µm dots were generated with a 12 µm Z-piezo extension in the same pen array configuration. This feature of PPL allows one to not only multiplex, but also span the sub-100 nm to many µm length scale in a single patterning experiment.

Additionally, the protein structures patterned by PPL maintain their biological activity. As a proof-of-concept experiment, we patterned 5 × 5 prostate specific antigen (PSA) dot arrays

by PPL onto a Codelink slide with increasing tip-substrate contact times and contact forces. The distances between neighboring dots (in one array) and neighboring arrays were 5 μm and 60 μm, respectively. This protein chip was labeled by its corresponding antibody by immersion in a PBS (pH 7.4) solution containing 100 nM Alexa Fluor 488 conjugated anti-PSA for 1 hr, followed by rinsing, drying and imaging with fluorescence microscopy. As shown in Figure 3d, anti-PSA binds selectively onto the PSA regions with undetectable background, indicating that PSA maintained its bioactivity through the PPL process. The feature size increases from 1.1 to 3.2 μm with increasing contact force. Interestingly, the fluorescence intensity increases with increasing tip-substrate contact time, most likely because of higher PSA densities at longer contact times.

In conclusion, we have demonstrated a novel way of using a PPL array mould to localize different inks on the pens of a PPL array. This new strategy for localizing the respective inks on the nanoscale tips of a two-dimensional PPL array allows for the multiplexed patterning of protein nano and micro arrays in a high throughput and low-cost manner. The resulting structures are bioactive and can be prepared with no evidence of cross-contamination over very large areas. This novel method is a general approach, which in principle can be applied to large scale, multiplexed nano- and micropatterning of many biomolecules and other libraries of small molecules, catalysts, and essentially any set of structures which can be transported by PPL.

A.4. Combinatorial Arrays Generated by Cantilever-Free Scanning Probe Lithography

Hard-Tip Soft-Spring Lithography

Polymer pen lithography (PPL) overcomes the fundamental throughput limitations imposed by the serial nature of scanning probe-based lithographic methods. While there are microfabrication techniques available for fabricating large-area arrays of AFM cantilevers for DPN, these approaches are expensive and produce fragile pen arrays that are difficult to align. By replacing the cantilever with an elastomeric backing layer and pen material, PPL retains the registration and throughput capabilities of 2-D DPN while dramatically lowering the cost and complexity in fabricating the pen arrays. However, the resolution of PPL is limited by the elastomeric nature of the tips, which typically have a diameter of 70 ± 10 nm. Last year, we developed a method for combining the strengths of DPN and PPL – high resolution, low cost and massively parallel architectures – by forming pen arrays that consist of hard Si tips attached to an elastomeric backing. The resulting technique, termed hard-tip, soft-spring lithography (HSL), is a cantilever-free technique that uses direct deposition of materials or energy onto a surface to create arbitrary patterns with sub-50 nm resolution over large areas.

The key innovation for HSL is a novel protocol (Fig. 25) for fabricating arrays of ultra-sharp Si on an elastomeric backing layer that allows all of the tips to be brought into contact with the surface at the same time. The array architecture consists of thousands of Si tips on a layer of elastomer, such as polydimethylsiloxane (PDMS), coated on a glass slide. In addition to lowering the cost of making these pen arrays, the transparency of the elastomeric backing allows one to use optical leveling to ensure all tips are in contact with the substrate.

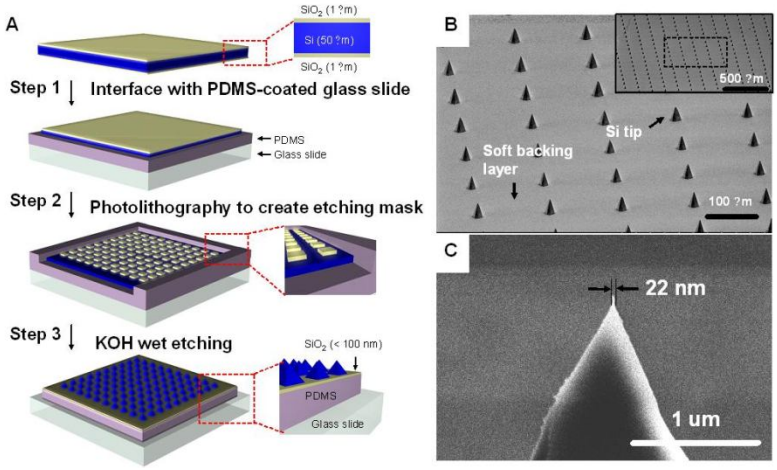

Figure 25. *(A) Schematics of the steps involved in fabricating a HSL tip array. (B) SEM image of a Si tip array on SiO2/PDMS/glass with a 150-μm pitch between tips. (C) SEM of individual ultrasharp tip with a 22 nm diameter.*

To make the tip arrays (Fig. 25A), a 1 cm^2 piece of a 50-μm-thick Si(100) wafer with a 1-μm-thick layer of SiO_2 on each side of the wafer was placed onto uncured PDMS. The top layer of the SiO_2 eventually serves as an etching mask, while the oxygen-plasma-treated bottom SiO_2 layer of the wafer in contact with the hydrophilic surface of the PDMS increases adhesion between the two surfaces, so that the tips do not fall off the array once the wafer has been etched. After the elastomer was cured, photolithography was used to define 150 μm^2 square features of exposed SiO2, each of which will be used to prepare an ultrasharp tip. It is important to note that, depending on the intended use, the pitch of the tip array can be varied by changing the photolithographic mask. The density can be as high as 110,000 tips/cm^2, which corresponds to ~9,000,000 tips on a 4-inch wafer. After photolithography, HF is used to remove the exposed SiO2, and an aqueous solution of KOH (40% w/v) at 75°C is used to anisotropically etch the underlying Si. After the etching step (60-65 min), the tip array was removed from the etchant, rinsed with water and dried under a nitrogen stream. If the backing layer is not flexible enough, further SiO_2 etching in HF can be conducted.

Uniformity of the tips across the array was confirmed by scanning electron microscopy (SEM) and optical microscopy (Fig. 25B). The architecture of the arrays – Si tips on a PDMS-coated glass slide – allows one to easily manipulate and mount the array onto an AFM scanner without damaging it. Importantly, SEM shows that the average tip height is 47 ± 0.9 μm. This small variation in height might cause a difference in tip-surface contact time of a few tens of milliseconds, but will not significantly vary the feature size because of the speed of z-piezo extension (100 μm/s). The resulting tip diameter is 22 ± 3 nm (Fig. 25C), which is considerably smaller than the tip diameter of elastomeric tips from PPL.

The patterning capabilities of HSL were evaluated by printing 16-mercaptohexadecanoic acid (MHA) and poly(ethylene glycol) (PEG) onto thermally-evaporated polycrystalline Au and hexamethyldisilazane-coated Si surfaces, respectively. The tip arrays were spin-coated with an ethanolic solution of the ink molecule and mounted onto an XE-150 platform (Park Systems) equipped with a tilting stage, environmental humidity control chamber, specialized scanning head and custom software that can control the dwell time, position and z-piezo extension for each feature in the pattern. Like PPL, the compression of the elastomeric backing indicates that

the tips are in contact with the surface, and this method is used to optically level the plane of the tip arrays with respect to the plane of the surface.

In DPN, precise control of feature diameter is achieved because the ink diffuses through the meniscus that forms between the tip and the surface, thereby resulting in a linear relationship between feature area and the square root of the dwell time. This same linear relationship was observed in the case of HSL (Fig. 26A). In addition to the relationship between contact time and feature size, PPL shows a linear relationship between the force between tip array and surface and the resulting feature edge length due to tip compression. In HSL, however, there is no such relationship (Fig. 26B) because the hard tips do not deform under pressure. This lack of feature diameter dependence on the array-substrate force suggests that all tips in HSL can be brought into contact by extending the z-piezo without consequences on the resulting feature sizes, even though the force exerted on each tip may differ. These results demonstrate that dwell time and humidity can be used to effectively control the resulting feature size from several micrometers to less than 50 nm.

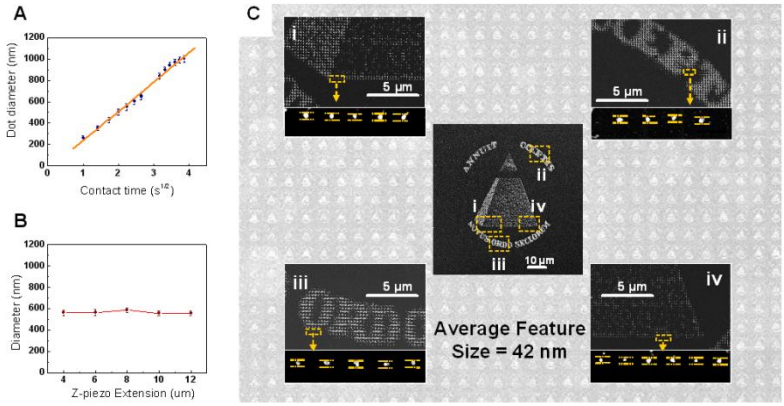

Figure 26. *(A) Relationship between contact time and resulting dot diameter. (B) Relationship between contact force and resulting dot diameter. Both (A) and (B) match observed trends traditional deposition by DPN. (C) Background is an optical micrograph demonstrating large area patterning of pyramids from US $1 banknote. Middle inset shows an SEM of a single pyramid pattern; (i)-(iv) are SEM images showing magnified views of the yellow boxes indicated in the middle inset. Each zoomed-in image has another SEM image below it showing size of individual spots from the pattern.*

By combining the benefits of DPN and PPL, HSL is able to print arbitrary patterns in a massively parallel, mask-free fashion with sub-50 nm resolution. This capability was demonstrated by using MHA to form patterns consisting of the pyramid on the US $1 bill, and subsequent etching of the nonpatterned areas (Fig. 26C). In this pattern, the tip–substrate contact time was kept constant at 0.01 s with 30% ambient humidity. A representative portion of the ~19,000 replicas (yield >99%) generated across the 1-cm^2 substrate show the quality and high resolution of this novel nanofabrication technique. Importantly, at the edge of the etched Au patterns (Fig. 26C), individual dots can be clearly seen, allowing us to determine the average feature diameter (41 ± 7 nm). The standard deviation of the etched Au dot diameters for features generated by HSL was 17% across the 1-cm2 area, which results from minor variations in surface etching, tip morphology, ink coating, and the polycrystallinity of the Au surface. The total time required to fabricate this large-area, high- resolution pattern was about 200 minutes.

In conclusion, we have demonstrated a novel lithographic technique that combines the resolution of DPN with the low cost, relative ease of fabrication, and high throughput of PPL. This technique, HSL, is capable of patterning 40-nm features over 1-cm^2 areas, and is easily scalable to much larger (4-inch wafer) scales.

Using Tilted Polymer Pen Arrays to Investigate Mesenchymal Stem Cell Differentiation

Previous observations have shown that pluripotent adult mesenchymal stem cells (MSCs) can differentiate into several cell types ranging from adipogenic to osteogenic fates, each having characteristically different focal adhesion sizes. These focal adhesions span the nanometer to micrometer scale and consequently, we hypothesized that the ability to control the focal adhesion size may guide MSC differentiation towards a specific lineage without the use of biochemical cues. To evaluate this idea, we investigated whether nanometer or micrometer extracellular matrix protein feature size and spacing affects MSC differentiation towards an osteogenic lineage. As a proof of concept, we have studied fibronectin, which is known to bind integrin receptors in cell membranes; these integrin receptors than interact with intracellular proteins such as vinculin and paxillin to form complexes termed focal adhesions.

We show that by tilting a single elastomeric pen array (square centimeter in area) in combination with PPL, one can create combinatorial patterns. Specifically, by intentionally tilting the polymer pen array about 0.01°, patterns having different feature sizes, but the same feature pitch (Fig. 27A) can be made. Uniform Au feature dimensions ranging from 475 nm to 1.2 μm are fabricated by etching areas not patterned with 16-mercaptohexadecanoic acid (MHA) and observed using SEM (Fig. 27A). At the same time, it is possible to use the polymer pen array to make homogeneous features (Fig. 27B). The etched pattern is used to confirm the quality of ink transfer in addition to feature size; the remaining unetched patterned substrate is passivated using a 1 mM ethanolic solution of hexa(ethylene glycol)-undecanethiol for 1 hour at room temperature to reduce non-specific protein adsorption. The substrate is rinsed with ethanol and dried with nitrogen before immersion in a 10 mM ethanolic solution of cobalt nitrate for 1 hour at room temperature. In this step, cobalt cations chelate the carboxylic acid groups in MHA, which enable selective orientation of fibronectin.

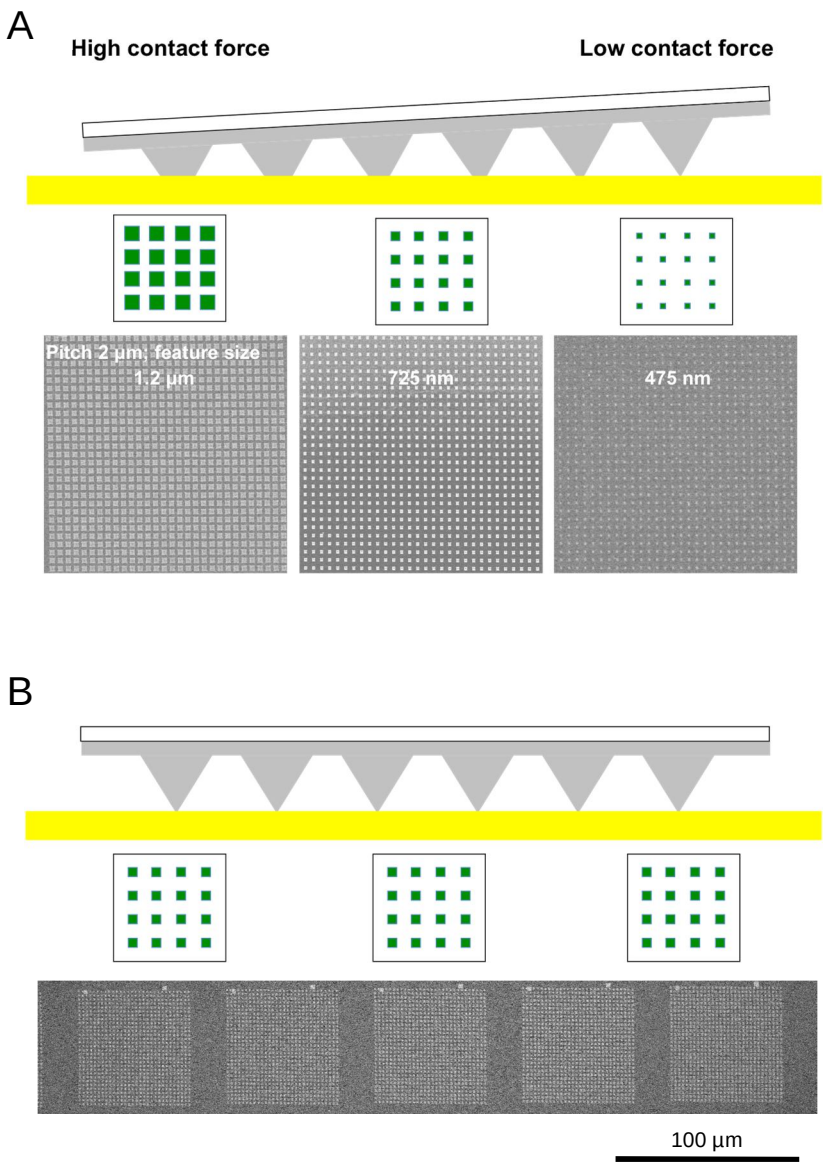

Figure 27. *(A) Scheme of tilting the polymer pen array to generate combinatorial libraries. Scanning electron micrograph (SEM) images of patterned MHA features on Au after chemical etching. (B) Scheme of using a level polymer pen array for making large area patterns. SEM image of uniform MHA features on Au after chemical etching.*

Human bone marrow-derived MSCs (Lonza) attach to the patterned areas and are cultured in the presence of normal growth media for one week. We have observed in preliminary work (Fig. 28) that when the total amount of fibronectin presented to each MSC is held constant, substrates consisting of 300 nm features promote the expression of osteogenic markers, alkaline phosphatase and osteocalcin, in MSCs to a greater extent than both unpatterned surfaces and substrates consisting of 1 µm scale features.

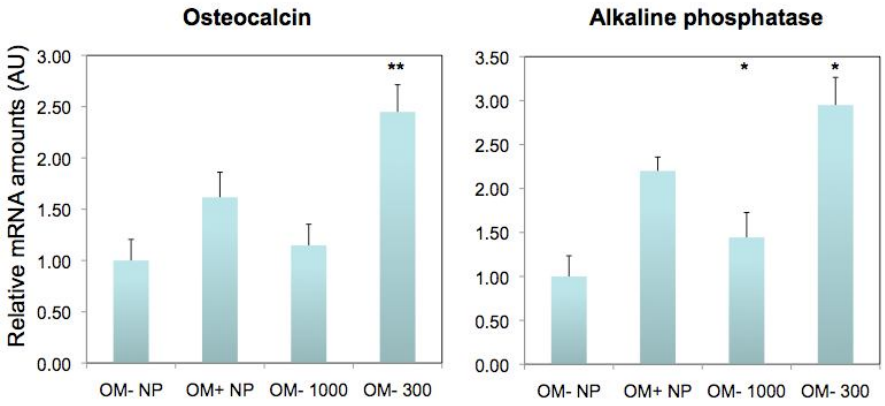

Figure 28. *RT-PCR results for relative mRNA expression levels of osteocalcin and alkalinephosphatase for MSCs grown in the absence of patterns and osteogenic media (OM- NP), absence of patterns but with osteogenic media (OM+ NP), and absence of osteogenic media with 1 μm patterns (OM- 1000) and 300 nm patterns (OM- 300).*

Beam-Pen Lithography (BPL)

Beam pen lithography is a technique that uses light incident on metal-coated PPL arrays to generate arbitrary patterns in a photoresist. In order to couple PPL with near-field optical lithography, conventional PPL arrays are coated with an ~80 nm layer of gold (5 nm Ti adhesion layer) that is optically opaque. To pattern the photoresist, it is necessary to form apertures at the tips of each pen, which is accomplished by bringing the array into contact with an adhesive poly(methyl methacrylate) (PMMA) surface (Fig. 29A). The average size of the aperture was varied from 500 nm to 5 μm by controlling the contact force between the BPL tip array and the PMMA-coated substrate. Additionally, focused ion beam (FIB) lithography was used to make apertures with diameters as small as 50 nm (Fig. 29B).

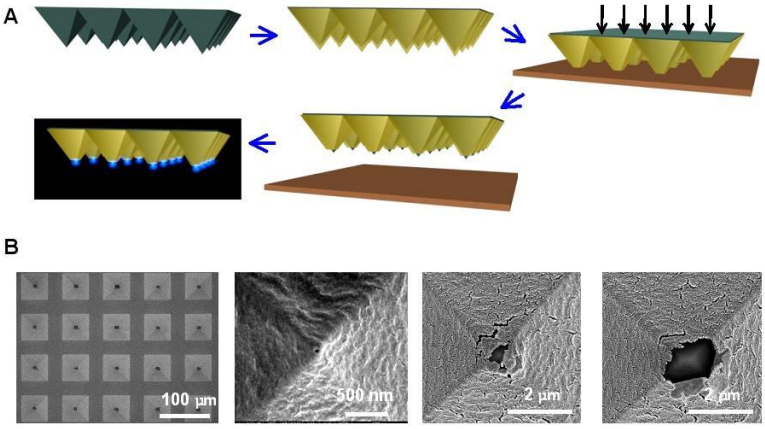

Figure 29. *(A) Schematic of the steps involved in fabricating apertures in a BPL tip array. (B) SEM of tip array after aperture fabrication. Images on the right are of tips with apertures that are 50 nm, 200 nm, and 1 μm from left to right, respectively.*

BPL experiments were performed using an AFM platform (XE-150, Park Systems Co.) that was customized for PPL. During a typical experiment, a 1 cm2 BPL array was brought into contact with a silicon surface that had been pre-coated with a layer of positive photoresist, followed by UV light exposure above the beam pen array (Fig. 30A). Due to the opaque nature of the gold layer, light was transmitted only through the apertures, resulting in the formation of a

single dot per tip for each light exposure. The diameter of each dot can be modulated both by aperture size and by varying a number of lithographic parameters, including resist type and resist layer thickness. For example, by using arrays with FIB-generated apertures (aperture diameter of 50 ± 5 nm), a 40-nm thick resist layer and a ~400 nm halogen light source to pattern the photoresist, followed by development, metal evaporation and photoresist lift-off, chromium features with diameter of 111 ± 11 nm were generated. These features are significantly smaller than that predicted by the diffraction limit.

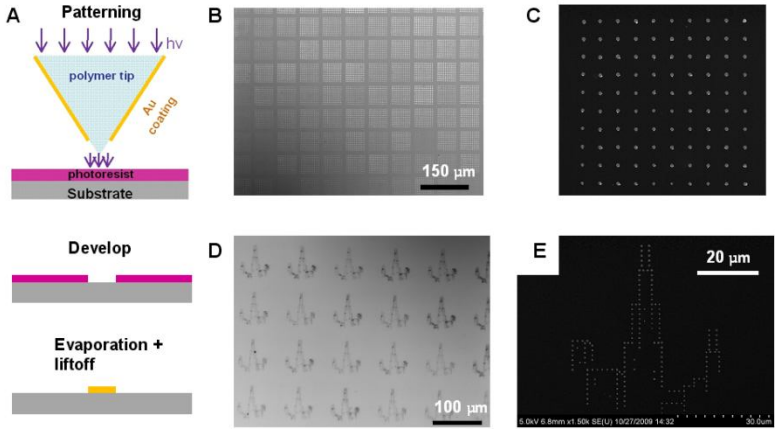

Figure 30. *(A) Schematic of individual tip during BPL, demonstrating exposure of select light-sensitive photoresist-coated regions. (B) Optical microscopy image of developed photoresist patterns. (C) SEM of single pattern from (B) of resulting gold dots. (D) Optical microscopy image of 182 gold dots in the shape of the Chicago skyline, demonstrating arbitrary patterning capability. (E) SEM of single pattern of the Chicago skyline from part (D).*

Massively parallel near-field optical lithography could be achieved by using PMMA to generate apertures in large area BPL arrays such that the average aperture diameter is 700 nm. Illumination of a 1 cm2 array allowed the generation of 15,000 patterns, where each pattern consisted of a 10 x 10 dot array, leading to a total of 1.5 million features generated in 30 minutes (Figs. 30B, C). The diameter of each dot after exposure (90% maximum power light intensity, 20 s exposure per dot), development, Au evaporation, and photoresist lift-off was 750 ± 80 nm. Because the light remains on for the duration of the experiment, lateral and vertical movement of the BPL array across the substrate was rapid (60 µm/sec) in order to avoid unwanted exposure.

The maskless nature of BPL allows generation of arbitrary patterns without the need for fabricating new masters. To demonstrate this concept, a BPL array with 500 nm apertures was used to make 15,000 copies of a 182-dot (20 s exposure per dot) pattern in the shape of the Chicago skyline (Figs. 30D, 30E). After metal evaporation and lift-off, the patterned dots were 450 ± 70 nm in diameter with 600 nm pitch.

BPL can also be used to address a significant challenge in scanning probe lithography methods; namely, addressing each tip so that individual tips write different patterns. While the tips are nanoscopic, the base of each tip is microscopic and thus easily addressable with light. In a proof-of-concept experiment, a chrome photomask was used to cover selected areas of the BPL array (Fig. 31A). Thus, when the light source was selectively illuminated on certain tips (e.g. in a "U" pattern – see Fig. 7B) with a photomask, only the illuminated tips exposed the underlying photoresist. No patterns were observed from unmasked tips.

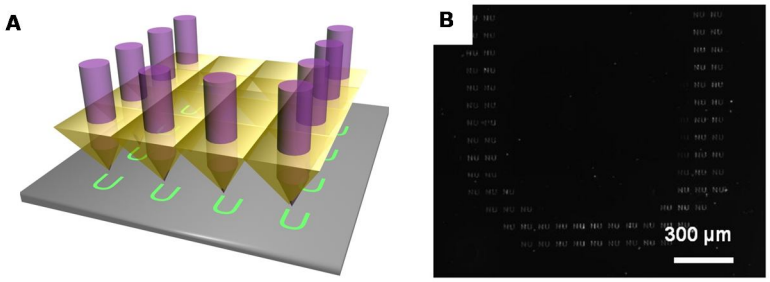

Figure 31. *(A) Schematic of addressing individual pens with light. (B) Scanning electron microscopy image showing selective illumination of the beam pen array with a mask in the shape of a "U" pattern as well as arbitrary nanoscale pattern generation (small "NU" patterns).*

In summary, our lab has developed a novel lithographic method that combines PPL arrays with near-field scanning optical microscopy methods by coating the sidewalls of each tip with an opaque metal layer. BPL can be readily combined with conventional photolithography methods, and the near-field alignment of the tips permits the generation of sub-diffraction limit feature sizes. Importantly, the combination of nanoscale tip movement for arbitrary pattern generation with macroscale selective illumination of desired pens provides a simple, flexible and low-cost tool that could be used for a number of biological studies because of its ability to generate complex patterns for rapid prototyping.

Scanning Probe Block Copolymer Lithography (SPBCL)

Due to their size-dependent optoelectronic and chemical properties, there is an increasing interest in synthesizing ordered arrays of single nanoparticles for applications ranging from biomedical sensors to single-electron transistors. Indeed, the precise positioning and synthesis of sub-10 nm particles over a large area is exceedingly difficult using current lithographic techniques, particularly those commonly available in an academic research lab. Toward this end, we developed a new high resolution scanning probe-based technique called scanning probe block copolymer lithography (SPBCL). In all SPBCL experiments, a block copolymer-based solution (Fig. 32A) was used as an ink for conventional DPN and PPL. A typical ink consisted of a solution of 0.5 wt% poly(ethylene oxide)-b¬-poly(2-vinylpyridine) (PEO-b-P2VP) in water. A metal salt, such as HAuCl4, was added to the block copolymer solution in a 2:1 molar ratio of pyridine:Au. The polymer used here, PEO-b-P2VP, was chosen because the PEO chains provide water solubility and the P2VP chains serve to concentrate the metal ions.

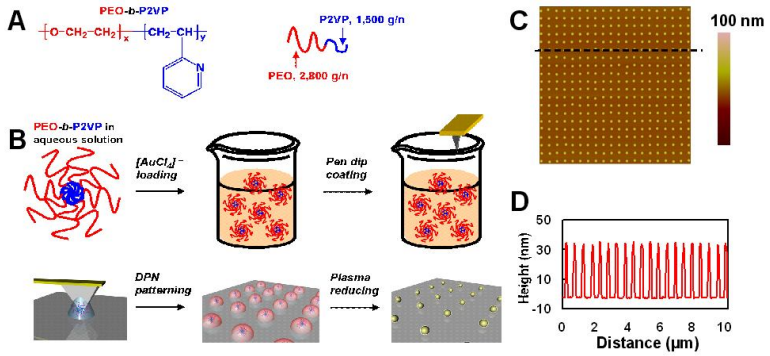

Figure 32. *(A) Structure of block copolymer used as ink material. (B) Schematic of the SPBCL process used to make individual gold nanparticles. (C) Atomic force micrograph of block copolymer spots on HMDS coated substrate. (D) Height profile of dashed line in (C).*

In a typical patterning experiment (Fig. 32B), the DPN tip array was dip-coated with the ink, dried under a N_2 stream, and placed into an NScriptor system (NanoInk, Skokie, IL). In order to facilitate transport of the viscous ink, patterning was done at high humidity (70-100%). The substrates used were a hexamethyldisilazane (HMDS)-coated Si/SiO_x surface for the AFM experiments, and a 50-nm-thick Si_3N_4 grid with hydrophobic coating (Ted Pella, Inc.) for the TEM experiments. To demonstrate facile patterning of small dot arrays, a square 10x10 array was patterned at 70% humidity using a 0.01 s dwell time, which yielded 90 ± 7 nm diameter dots (Figs. 32C and 32D). After plasma treatment, the precursor spots yielded square arrays of sub-10 nm gold nanoparticles, as shown by XPS and SEM.

In order to verify the crystallinity of the nanoparticles and investigate the relationship between precursor spot size (determined by humidity and dwell time) and final nanoparticle size, arrays of spots were printed onto a TEM grid using a variety of dwell times under a saturated atmosphere. The precursor spot patterns followed the relationship already established for DPN, where the feature dimension is linearly related to the square root of the tip-substrate contact time (Fig. 9A). After plasma treatment, the nanoparticles (Figs. 33B and 33C) had a diameter ~10x smaller than the block copolymer spots. By adjusting the concentration of pyridine:Au from 2:1 to 4:1, the NP diameter was used to reduce the average particle diameter to 4.8 ± 0.2 nm.

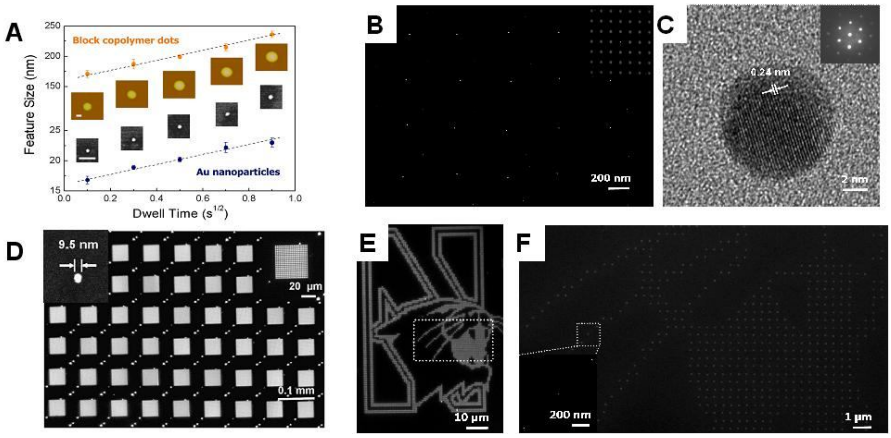

Figure 33. *(A) Relationship between dwell time and feature size for polymer spots (top line) and nanoparticles (bottom line). (B) SEM of sub-10 nm Au nanoparticles formed after plasma treatment. Inset is a Fourier transform of the image. (C) High resolution TEM image showing an 8-nm diameter single-crystalline Au nanoparticle. The measured lattice spacing is 0.24 nm. Inset shows a typical electron diffraction pattern from an Au(111) nanoparticle. (D) Dark field (DF) optical micrograph of large area patterns polymer patterns formed by PPL. Right-hand inset shows an image of a single pattern; left-hand inset shows size of single nanoparticle after plasma treatment. (E) DF micrograph of Northwestern University wildcat logo made of individual precursor spots. (F) SEM image of grey box in E after plasma treatment, showing individual nanoparticles. Inset is an SEM image of a single gold nanoparticle.*

In order to make large-area patterns of sub-10 nm nanoparticles, SPBCL was used in conjunction with PPL. As a proof-of-concept demonstration, a 1 cm2 PPL array was inked with the PEO-b-P2VP/AuCl4- ink by spin-coating. The patterning was performed on a customized AFM

platform (Park XEP, Park Systems Co.) at 80% humidity, and each pen was used to write a 20x20 square pattern of dots (Fig. 33D). Because of the short dwell time (0.5 s), the entire patterning process generated 25 million features in less than 5 minutes. Like all SPL techniques, there is no need to fabricate a mask and thus arbitrary patterns can be generated. To demonstrate this, a pattern of sub-10 nm Au nanoparticles was written in shape of the Northwestern University wildcat logo (Figs. 33E, F).

Inking PPL arrays with a block copolymer/metal salt-based ink permits a number of combinatorial studies to be conducted. In particular, deliberate tilting of the PPL array with respect to the substrate will generate a series of feature sizes across the substrate (Fig. 34A). For instance, tilting a 1-cm^2 PPL array by 0.01° results in the generation of block copolymer features with diameter ranging from 200-600 nm (Figs. 34B, 34C). After annealing, these arrays yield NPs ranging in size from 15-50 nm (Fig. 34D). Since the feature size in PPL-generated patterns can be varied by changing both dwell time and tip-substrate force, there are a number of parameters that can be used to control the resulting feature size in a combinatorial fashion. For combinatorial studies, it is important that SPBCL be generalized to other metal systems for novel applications in electronics, magnetics and catalysis. Toward this end, our group has so far demonstrated SPBCL with both Pt and Fe.

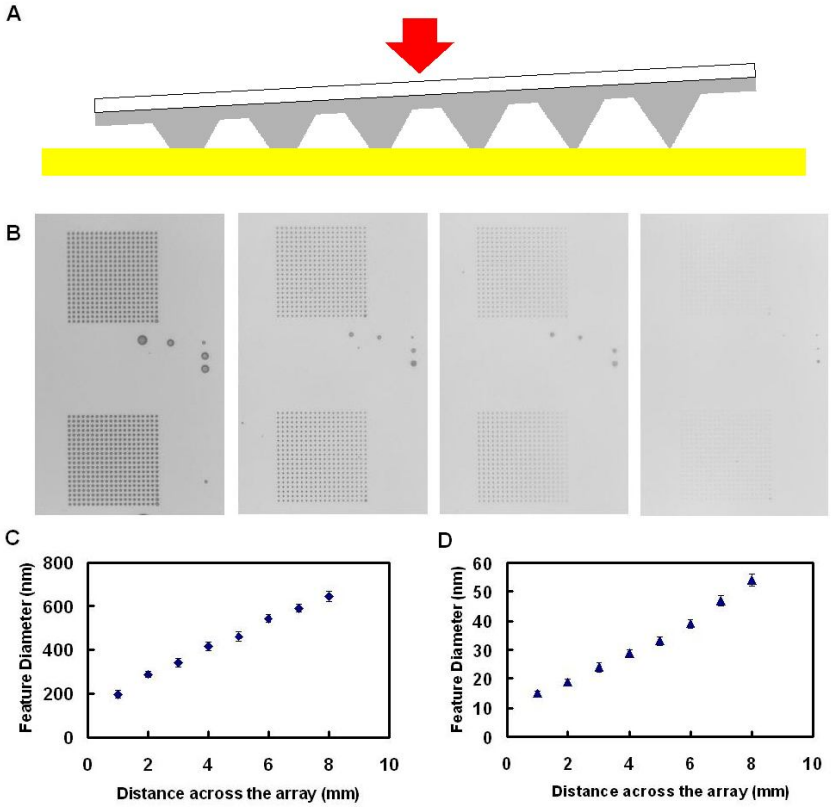

Figure 34. *(A) Schematic of tilting the pen array in relation to the substrate to generate combinatorial libraries of feature sizes. (B) Optical micrograph of block copolymer spots fabricated by tilting the array by 0.01°. Images from left to right are taken 2, 4, 6, and 8 mm away (respectively) from the tips that are closest to the surface. (C) Relationship between distance across the array and precursor feature diameter. (D) Relationship between distance across the array and final NP diameter.*

In conclusion, we have demonstrated a facile method for the synthesis of sub-10 nm metal nanoparticles, with high precision control over NP diameter and position. By deliberately tilting the PPL array, these metal NPs can be synthesized in a combinatorial fashion. By extending this work to yet more materials, the technique of SPBCL enables a number of studies in magnetics, optoelectronics, and catalysis to be performed. Additionally, this technique enables fundamental studies because metal nanoparticles are about the size of a single protein. Using the correct attachment chemistry, we envision using SPBCL to template the patterns of individual proteins.

B. PERSONNEL SUPPORTED

Postdocs	**Percentage of Salary Provided by Grant**
Zijian Zheng	100%
Gengfeng Zheng	25%
Adam Braunschweig	unfunded
Lu Shin Wong	unfunded

Graduate Students	**Percentage of Salary Provided by Grant**
Boris Rasin	100%
Peng Sun	75%
Wooyoung Shim	50%
Shu He	50%
Naoyuki Shimazu	55%
Charles Machan	35%
Mari Rosen	35%
Tuncay Ozel	35%
Bryan Mangelson	25%
Daniel Eichelsdoerfer	unfunded
Louise Giam	unfunded

C. PUBLICATIONS

1. Sanedrin, R. G.; Huang, L.; Jang, J.-W.; Kakkassery, J.; Mirkin, C. A. “Polyethylene Glycol as a Novel Resist and Sacrificial Material for Generating Positive and Negative Nanostructures,“ *Small* **2008**, *4*, 920-924.
2. Jang, J.-W.; Sanedrin, R.; Maspoch, D.; Hwang, S.; Fujigaya, T.; Jeon, Y.-M.; Vega, R.; Chen, X.; Mirkin, C. A. ”Electrically Biased Nanolithography with KOH Coated AFM Tips,” *Nano Lett.* **2008**, *8*, 1451-1455.
3. Wang, Y.; Giam, L. R.; Park, M.; Lenhert, S.; Fuchs, H.; Mirkin, C. A. “A Self-Correcting Inking Strategy for Cantilever Arrays Addressed by an Inkjet printer and Used for Dip-Pen Nanolithography,” *Small* **2008**, *4*, 1666-1670.
4. Huo, F.; Zheng, Z.; Zheng, G.; Giam, L. R.; Zhang, H.; Mirkin, C. A. “Polymer Pen Lithography,” *Science* **2008**, *231*, 1658-1660.
5. Zheng, Z.; Jang, J.-W.; Zheng, G.; Mirkin, C. A. “Topographically Flat, Chemically, Patterned PDMS Stamps Made by Dip-Pen Nanolithography,” *Angew. Chem. Int. Ed.* **2008**, *47*, 9951-9954.
6. Giam, L. R.; Wang, Y.; Mirkin, C. A. “Nanoscale Molecular Transport: The Case of Dip-

Pen Nanolithography," *J. Phys. Chem A* **2009**, 113, 3779–3782.
7. Braunschweig, A. B.; Senesi, A. J.; Mirkin, C. A. "Redox-Activating Dip-Pen Nanolithography (RA-DPN)," *J. Am. Chem. Soc.* **2009**, *131*, 922-923.
8. Braunschweig, A. B.; Huo, F.; Mirkin, C. A. "Molecular Printing," *Nature Chemistry* **2009**, 1, 353 – 358.
9. Jang. J.-W.; Sanedrin, R. G.; Senesi, A.; Zheng, Z.; Chen, X.; Hwang, S.; Huang, L.; Mirkin, C. A. "Dip-Pen Nanolithography Generated Metal Photomasks," *Small* **2009**, 5, 1850–1853.
10. Zheng, Z. J.; Daniel, W. L.; Giam, L. R.; Huo, F.; Senesi. A. J.; Zheng, G.; Mirkin, C. A. "Multiplexed Protein Arrays Enabled by Polymer Pen Lithography: Addressing the Inking Challenge," *Angew. Chem Int. Ed.,* **2009,** *48,* 7626-7629.
11. Senesi, A. J.; Rozkiewicz, D. I.; Reinhoudt, D. N.; Mirkin, C. A. "Agarose-Assisted Dip-Pen Nanolithography of Oligonucleotides and Proteins," *ACS Nano* **2009**, *3*, 2394-2402.
12. Liao, Xing; Braunschweig Adam; Mirkin, C. A. "Force-Feedback" Leveling of massively parallel arrays in polymer pen lithography," *Nano Letters*, **2009**, 10, 1335-1340.
13. Huang, L.; Braunschweig, A. B.; Shim, W.; Qin, L.; Lim, J.-L.; Hurst, S.; Huo, F.; Xue, C.; Jang, J.-W.; Mirkin, C. A. "Matrix-Assisted Dip-Pen Nanolithography (MA-DPN) and Polymer Pen Lithography (MA-PPL)," Small **2010**, 6, 1077-1081.
14. Liao, X.; Braunschweig, A. B.; Zheng, Z.; Mirkin, C. A. "Force- and Time-Dependent Feature Size Control on Molecular Printing via Polymer Pen Lithography (PPL)," Small **2010**, 6, 1082-1086.
15. Huo, F.; Zheng, G.; Liao, X.; Giam, L. R.; Chai, J.; Chen, X.; Shim, W.; Mirkin, C. A. "Beam Pen Lithography," Nature Nanotechnology, **2010**, 5, 637-640.
16. Chai, J.; Huo, F.; Zheng, Z.; Giam. L. R.; Shim, W.; Mirkin, C. A. "Scanning probe block copolymer lithography," PNAS, **2010**, 107, 20202-20206.
17. Salaita, K.; Amarnath, A.; Higgins, T. B.; Mirkin, C. A. "The Effects of Organic Vapor on Alkanethiol Deposition via Dip-Pen Nanolithography," Scanning, **2010**, 32, 9-14.
18. Jang, J. W.; Zheng, Z.; Lee, O.-S.; Shim, W.; Zheng, G.; Schatz, G. C.; and Mirkin, C. A. "Arrays of nanoscale lenses for subwavelength optical lithography," Nano Letters, **2010**, 10, 4399–4404.
19. Shim, W.; Braunschweig, A. B.; Liao, X.; Chai, J.; Lim, J. K.; Zheng, G.; Mirkin, C. A. "Hard-Tip, Soft-Spring Lithography," Nature, **2010**, 469, 516-520.
20. Chai, J.; Wong, L. S.; Giam, L. R.; Mirkin, C. A.; "Single-molecule protein arrays enabled by scanning probe block copolymer lithography," PNAS, **2011**, 108, 19521-19525.
21. Giam, L. R.; Mirkin, C. A. "Cantilever-free Scanning Probe Molecular Printing," *Angew. Chem. Intl. Ed.*, **2011**, *33*, 7482-7485.
22. Giam, L. R.; Massich, M. D.; Hao, L.; Wong, L. S.; Mader, C. C.; Mirkin, C. A. "Scanning probe-enabled nanocombinatorics: fibronectin feature size controls stem cell fate," PNAS, **2012**, doi: 10.1073/pnas.1201086109.
23. Wong, L. S.; Karthikeyan, C. V.; Eichelsdoerfer, D. J.; Micklefield, J.; Mirkin, C. A.; "A methodology for preparing nanostructured biomolecular interfaces with high enzymatic activity," Nanoscale **2012**, 4, 659-666.

D. PRESENTATIONS

1. 2008 AFOSR Biomimetic, Biomaterial and Biointerfacial Sciences Program Review, Key West, FL; "Diatomaceous, Fungal and Bacterial Building Blocks in Material Synthesis" and "Bioinspired Supramaolecular Enzymatic Systems (2008).
2. 21st Annual International Symposium, Center for Gene Structure and Function, Hunter College, New York, NY; "The Oligonucleotide Nanoparticle Conjugate and the Antisense Nanoparticle" (2008).
3. University of California – Berkeley, Department of Chemistry, Berkeley, CA; "Nanostructures in Biodiagnostics and Gene Therapy" (2008).
4. Edgar Fahs Smith Lecture, University of Pennsylvania, Department of Chemistry, Philadelphia, PA; "DNA Rules: Materials Synthesis, Biodiagnostics, and Intracellular Gene Regulation," (2008).
5. ICREA+ICIQ Conference on Supramolecular Approaches to Catalysis, Barcelona, Spain; Plenary Lecture "Allosteric Enzyme Mimics Realized through Coordination Chemistry," (2008).
6. Pittcon Conference, New Orleans, LA; "Nanoflares: Probes for Transfection, RNA Visualization, and Detection," (2008).
7. ACS Spring Meeting, New Orleans, LA; "Amorphous Infinite Coordination Polymer Nano-and Microparticles," (2008).
8. Frontiers of Cancer Nanotechnology Seminar Series Distinguished Lecturer, Emory University – Georgia Institute of Technology, Atlanta, GA; "The Polyvalent Oligonucleotide Nanoparticle Conjugate: A New Frontier in *In Vitro* Diagnostics and Intracellular Gene Regulation," (2008).
9. Department of Chemistry, Georgia State University, Atlanta, GA; "The Polyvalent Oligonucleotide Nanoparticle Conjugate: A New Frontier in *In Vitro* Diagnostics and Intracellular Gene Regulation," (2008).
10. Department of Chemistry, Georgia Institute of Technology, Atlanta, GA; "The Polyvalent Oligonucleotide Nanoparticle Conjugate: A New Frontier in *In Vitro* Diagnostics and Intracellular Gene Regulation," (2008).
11. Office of Naval Research, Technical Review, Arlington, VA; "Chemical and Physical Properties of Nanoprisms," and "Encoded Materials From Infinite Coordination Polymer Nanoparticles," (2008).
12. Rheinisch Westfaelische Technische Hochschule (RWTH), Department of Chemistry, Aachen, Germany; "DNA Rules: Materials Synthesis, Biodiagnostics, and Intracellular Gene Regulation," (2008).
13. Forschungszentrum (FZK) Karlsruhe, Karlsruhe, Germany; "Unconventional Nanofabrication Methods," (2008).
14. Bunsentagung 2008, Deutsche Bunsen-Gesellschaft fuer Physikalische Chemie, Saarbruecken, Germany; Pleanary Lecture "Dip-Pen Nanolithography," (2008).
15. Tip-Based Nanofabrication Kick-Off Meeting, Albuquerque, NM; "Scanning Probe Epitaxy," (2008).
16. NSTI Nanotechnology 2008 Conference, Boston, MA; Keynote "A Decade of Dip-Pen Nanolithography: Capabilities, Applications, and Future Challenges" (2008).
17. Gordon Research Conference ""Metals in Medicine", Procter Academy, NH; "The Polyvalent Oligonucleotide Nanoparticle Conjugate Applications in Biodiagnostics and Medicine" (2008).

18. DOE Nano ES & H Workshop "Safe Handling of Engineered Nanoscale Materials," Argonne National Laboratory, Argonne, IL; "Looking Forward to Nanotechnology" (2008).
19. Gordon Research Conference "Inorganic Chemistry", Salve Regina University, Newport, RI; "Allosteric Supramolecular Enzyme Mimics" (2008).
20. 236th ACS National Meeting, Philadelphia, PA; "Signal and Target Amplification via a Cascade Reaction Triggered by a Small Molecule Reaction with a Supramolecular Allosteric Enzyme Mimic" (2008).
21. 236th ACS National Meeting, Philadelphia, PA; "On-Wire Lithography" (2008).
22. 236th ACS National Meeting, Philadelphia, PA; "DNA Rules: Materials Synthesis, Biodiagnostics, and Intracellular Gene Regulation" (2008).
23. Nanyang Technological University, School of Materials Science and Engineering, Singapore; "Commercializing Advances in Nanotechnology: Challenges and Opportunities," and "DNA Rules: Materials Synthesis, Biodiagnostics, and Intracellular Gene Regulation" (2008).
24. NCI Nanotechnology Alliance Investigator Meeting, Chicago, IL; "Nanostructures in Medicine" (2008).
25. Center for Cancer Nanotechnology Excellence (CCNE) Annual Meeting, Northwestern University, Evanston, IL; "Development of Barcode Assays for the Detection of Ovarian and Prostate Cancer" (2008).
26. 23rd Annual Volwiler Science Lecture, Lake Forest College, Lake Forest, IL; "Small Things, Big Implications" (2008).
27. Biomedical Engineering Society Fall Meeting, Distinguished Achievement Award Lecture, St. Louis, MO; "Nanostructures in Medicine" (2008).
28. GoNano, Geoff Ozin's 65th Birthday Celebration, University of Toronto, Toronto, Canada; "Polymer Pen Lithography" (2008).
29. Symposium "A Celebration of Nano and Molecular Medicine", Institute of Nano and Molecular Medicine, University of Missouri, Columbia, MO; "DNA Rules: Materials Synthesis, Biodiagnostics, and Intracellular Gene Regulation" (2008).
30. DARPA/DSRC Workshop on "Nanomanufacturing with Molecular Recognition", School of Engineering & Applied Sciences, Harvard University, Cambridge, MA; "Physical & Chemical Approaches to Nanofabrication through Molecular Recognition" (2008).
31. Department of Materials Science & Engineering, University of Michigan, Ann Arbor, MI; "Unconventional Forms of Nanofabrication" (2008).
32. CCNE Nanobiotechnology Series, Department of Radiology, School of Medicine, Stanford University, Stanford, CA; "Nanostructures in Medicine" (2008).
33. Materials Research Society Fall Meeting, Session: Nanotechnology for Biomedical Applications, Boston, MA; "Nanoparticles as Gene Regulation Materials" (2008).
34. AFOSR 231DX & EX Natural Materials, Systems, and Extremophiles Review, Arlington, VA; "MURI: Bioinspired Supramolecular Enzymatic Systems," and "DPN-Generated Combinatorial Libraries" (2009).
35. 2009 The Society of Photo-Optical Instrumentation Engineers MOEMS – MEMS Symposium, San Jose, CA; Plenary Lecture "Massively Parallel Soft Pen Nanolithography" (2009).
36. California NanoSystems Institute (CNSI), University of California – Los Angeles, Los Angeles, CA; "Nanostructures in Biology and Medicine" (2009).

37. Pittcon Conference, Chicago, IL; "Nanodisk Codes and Multiplexed Detection via Raman Spectroscopy," "Nanostructures in Biodiagnostics," and Pittsburgh Analytical Chemistry Award lecture "Nanostructured Probes for Intracellular Gene Regulation and Diagnostics" (2009).
38. Hybrid Materials Conference, Vinci International Convention Center, Tours, France; "Unconventional Forms of Nanofabrication" (2009).
39. 237th ACS National Meeting, Salt Lake City, UT; "On Wire Lithography", "Anisotropic Noble Metal Nanostructures", and "Allosteric Supramolecular Systems" (2009).
40. Gustavus John Esselen Award for Chemistry in the Public Interest, American Chemical Society, Cambridge, MA, "Nanostructures in Chemistry, Biology, and Medicine: Realized Promise and Future Prospects," (2009).
41. Tip-Based Nanofabrication PI Review Meeting, New Orleans; "Scanning Probe Epitaxy," (2009).
42. 100th American Association for Cancer Research (AACR) Annual Meeting, Denver, CO; "Cancer Diagnostics Using Nanotechnology Platforms" and "High Sensitivity Cancer Screening Tools Based upon Inorganic Nanostructures," (2009).
43. Joseph Priestley Lecture, Department of Chemistry, Pennsylvania State University, University Park, PA; "Programming Materials Synthesis with DNA: Applications in Biology and Medicine," (2009).
44. Colloquium, Department of Chemistry, Pennsylvania State University, University Park, PA; "Anisotropic Nanostructures: Building Valency into Nanoparticles," (2009).
45. Max T. Rodgers Distinguished Lecture, Department of Chemistry, Michigan State University, East Lansing, MI; "Programming DNA Synthesis with DNA – Applications in Biology and Medicine" and "Anisotropic Nanostructures – Building Valency into Nanoparticles," (2009).
46. Fred Pattison Lectures, Department of Western Ontario, London, ON, Canada; "DNA Rules: Materials Synthesis, Biodiagnostics, and Intracellular Gene Regulation", "Anisotropic Nanostructures: Building Valency into Nanoparticles," and "A Coordination Chemistry Approach to Supramolecular Enzyme Mimics," (2009).
47. McLean Lectures, Department of Chemistry, McMaster University, Hamilton, ON, Canada; "DNA Rules: Materials Synthesis, Biodiagnostics, and Intracellular Gene Regulation", and "Anisotropic Nanostructures: Building Valency into Nanoparticles," (2009).
48. ACS Great Lakes Regional Meeting, Lincolnshire, IL; "Nanoparticle-Based Intracellular Gene Regulation and Detection," (2009).
49. National Defense Education Program (NDEP) Research & Education Conference, NSSEFF, Arlington, VA; "Functional One Dimensional Structures Based Upon On-Wire Lithography," (2009).
50. Robert F. Rushmer Lecture, Department of Bioengineering, University of Washington, Seattle, WA; "Nanostructures in Biology and Medicine – Transitioning Novel Diagnostics and Therapeutic Tools from the Bench to the Clinic," (2009).
51. Plenary Lecture, 41st National Organic Symposium, Denver CO; "Programming Materials with DNA – Applications in Biology and Medicine," (2009).
52. Plenary Speaker, ICMAT 2009 - International Conference on Materials for Advanced Technologies, Materials Research Society – Singapore, Singapore; "Nanostructures in Biodiagnostics and Therapeutics," (2009).
53. DARPA – MEMS PI Meeting, SunRiver, OR; "Scanning Probe Epitaxy," (2009)

54. 238th ACS National Meeting, Washington, D.C.; "Nanostructures in Medicine and Biology" and "Nanostructures as Labels and Taggants in High Sensitivity Detection and Encoding Systems," (2009).
55. Bio-X Taggant Review, Dayton, OH; "Plasmonic Encoding," (2009).
56. 6th Key Symposium on Nanomedicine, Stockholm, Sweden; "Polyvalent Nucleic Acid Nanoconjugates in Materials Synthesis, Biodiagnostics, and Intracellular Gene Regulation," (2009).
57. NIH Director's Pioneer Award Symposium, Bethesda, MD; "Nanostructures for Problems in Biology," (2009).
58. Micro-and NanoEngineering Conference, Ghent, Belgium, "Unconventional Approaches to Nanofabrication," (2009).
59. Havinga Medal, Leiden University, Amsterdam, The Netherlands; "Programming the Assembly of Inorganic Materials with DNA: Applications in Biology and Medicine," (2009).
60. NCI Nanotechnology Alliance Investigators Meeting, Manhattan Beach, CA; "Role of PCAST in Science," (2009).
61. UOP-Honeywell, Des Plaines, IL; "Unconventional Approaches to Nanofabrication," (2009).
62. Society of Analytical Chemists of Pittsburgh, Pittsburgh, PA; "Nanostructures in Biology and Medicine," (2009).
63. University of Pittsburgh, PA; "Anistropic Nanostructures: Building Valency into Nanoparticles," (2009).
64. Arnold C. Ott Lecture, Grand Valley State University, Allendale, MI; "Building Valency in Metallic Nanostructures: The Atom Analogy" and "Programming Materials Assembly with DNA: Applications in Biology and Medicine," (2009).
65. Chemical and Biological Defense Science and Technology Conference, Dallas, TX; "Nanostructures in Biology and Medicine," (2009).
66. Fred Kavli Lecture, Materials Research Society, Boston, MA; "Massively Parallel Polymer Pen Lithography," "Rationally Designed Nanostructures Fabricated by On-Wire Lithography," and "The Polyvalent Gold Nanoparticle Conjugate: Materials Synthesis, Biodiagnostics, and Intracellular Gene Regulation," (2009).
67. NSF Nanoscale Science and Engineering Grantees Conference, Arlington, VA; "A PCAST Perspective on Nanotechnology Development," (2009).
68. Ohio State University, Columbus, OH; "Programming Materials Synthesis with DNA: Applications in Biology and Medicine," and "Unconventional Approaches to Nanofabrication," (2010).
69. Pittcon Conference, Orlando, FL; "Multiplexed Detection with Nanodisk Codes," and "Nanoflares: A New Modality in Biodiagnostics and Bioimaging," (2010).
70. 237th ACS National Meeting, San Francisco, CA; "Nanoflares for the Intracellular Detection of Small Molecules, Nucleic Acids, Metal Ions, and Protein Targets," and "Anisotropic Nobel Metal Nanostructures," (2010).
71. University of California – Berkeley, Berkeley, CA; "Programming the Assembly of Nanoparticles with DNA: The Atom Analogy," (2010).
72. Herman S. Bloch Memorial Lecture, University of Chicago, Chicago, IL; "Molecular Printing: A Chemist's Approach to Desk Top Fab," (2010).

73. 101st American Association for Cancer Research (AACR) Annual Meeting, Washington, DC; "The Polyvalient Nanoparticle Conjugate: A New Frontier in Cancer Diagnostics and Therapeutics," (2010).
74. James Madison University, Harrisonburg, VA; "Nanotechnology: Small Wonders, Medical Miracles," (2010).
75. University of Kentucky, Lexington, KY; "Programming Materials Synthesis with DNA: Applications in Biology and Medicine," (2010).
76. Digestive Disease Week for Society for Surgery of the Alimentary Tract, New Orleans, LA; "Nanotechnology in Biology and Medicine," (2010).
77. 54th International Conference on Electron, Ion, & Proton Beam Technology & Nanofabrication, Anchorage, Alaska; "Molecular Printing: A Chemist's Approach to a Desk Top Fab," (2010).
78. Gordon Research Conference on Noble Metal Nanoparticles, Mount Holyoke College, South Hadley, MA; Alexander M. Cruickshank Lecture on "Nanoparticle Bioconjugates: A New Frontier in Materials Science, Biology, and Medicine," (2010).
79. Gordon Research Conference on Plasmonics, Colby College, Waterville, Maine; "Chemical Approaches to Making Plasmonically Active Nanostructures," (2010).
80. ACS National Meeting, Boston, MA, "Towards a Desktop Fab: Polymer Pen Lithography and Beam Pen Lithography," "DNA-Programmable Assembly of Colloidal Crystals," "Nanoflares: A New Modality in Biodiagnostics and Bioimaging," and "Oligonucleiotide-Gold Nanoparticles Conjugates as Intracellular Gene Regulation Agents," (2010).
81. IEEE Nano 2010 / Nano Korea 2010, Seoul, Korea, "Molecular Printing: A Chemist's Approach to Desktop Fab," (2010).
82. University of Calgary, Calgary, Alberta, Canada, "The Polyvalent Gold Nanoparticle Conjugate: Materials Synthesis, Biodiagnostics, and Intracellular Gene Regulation," and "Molecular Printing: A Chemist's Approach to a Desk Top Fab," (2010).
83. Scripps Research Institute, La Jolla, CA, "Polyvalent DNA: A New Frontier in Molecular Diagnostics and Intracellular Gene Regulation," (2010).
84. The Pennsylvania State University, State College, PA, "Polyvalent DNA Nanostructures: A New Frontier in Materials Synthesis, Biodiagnostics, and Intracellular Gene Regulation," (2010).
85. Materials Research Society Fall Meeting, Boston, MA, "Oligonucleotide-Gold Nanoparticle Conjugates as Probes for Intracelluar Diagnostics and Gene Regulation," (2010).
86. Einstein Award Lecture, Chinese Academy of Sciences, Beijing, China, "The Polyvalent Oligonucleotide Nanoparticle Conjugate: A New Frontier in Materials Synthesis, In Vitro Diagnostics, and Intracellular Gene Regulation," (2010).
87. Xiamen University, Xiamen, China, "Plasmonic Seeds: a Novel Strategy for Synthesizing Anisotropic Nobel Metal Nanostructures," (2010).
88. Pacifichem, Honolulu, HI, "Nanostructure Synthesis with Plasmonic Seeds", "Coordination-Based Abiotic Molecular Machines", and "Novel Forms of Biolabeling and Amplification Afforded by Structures Generated by On-Wire Lithography," (2010).
89. Gordon Research Conference, Ventura, CA, "Scanning Probe Block Copolymer Lithography," (2011).
90. AACR, Miami, FL, "Polyvalent DNA Nanostructures: New Modalities in Cancer Diagnostics and Therapeutics," (2011).

91. University of New Mexico, Chemistry Department Colloquium, Albuquerque, NM, "The Polyvalent Gold Nanoparticle Conjugate: Materials Synthesis, Biodiagnostics, and Intracellular Gene Regulation," (2011).
92. Sandia National Labs, Truman Lecture, Albuquerque, NM, "Molecular Printing: A Chemist's Approach a Desk Top Fab," (2011).
93. Lab Automation Conference, Palm Springs, CA, "The Polyvalent Oligonucleotide Nanoparticle Conjugate: A New Frontier in In Vitro Diagnostics and Intracellular Gene Regulation," (2011).
94. Pittcon Conference, Atlanta, GA, "Polyvalent DNA Architecture: New Modalities for Intracellular Gene Regulation and Detection" (Plenary Lecture), and "Intracellular Detection by Nano-Flares," (2011).
95. American Academy of Allergy, Asthma & Immunology Annual Meeting, San Francisco, CA, "Polyvalent DNA: A New Paradigm in Molecular Diagnostics and Intracellular Gene Regulation," (2011).
96. American Association for Cancer Research Annual Meeting, Orlando, FL, "Ultrasensitive Approaches to the Early Detection of Cancer," (2011).
97. National Institute of Standards and Technology, Gaithersburg, MD, "The Polyvalent Gold Nanoparticle Conjugate: Material Synthesis, Biodiagnostics, and Intracellular Gene Regulation," (2011).
98. University of Illinois at Champaign-Urbana, Chemistry Department Seminar, Urbana, IL, "Polyvalent Nucleic Acids Nanostructures for Detection and Intracellular Gene Regulation" (2011).
99. NUtech Ventures, Annual Innovator's Dinner, Lincoln, NE, "Innovation in Nanotechnology: Separating Hype from Real Opportunity," (2011).
100. 10^{th} US-Korea Workshop on Nanostructured Materials, 8^{th} US-Korea Workshop on Nanoelectronics, and NBIT Program Review, Gyeongiu, Korea, "Massively Parallel Nanostructure Assembly," (2011).
101. Technologies for Future Micro Nano Manufacturing, Napa Valley, CA, "The Evolution of Scanning Probe Molecular Printing" (2011).
102. ACS National Meeting, Denver, CO, "Plasmon-Mediated Syntheses of Silver Nanostructures" (2011).
103. Bio-X STT-TAGGANTS Review, Dayton, OH, "Biobarcodes and Nanoflares: New Nanotechnological Taggant Approaches" (2011).
104. Wright State University, Dayton, OH, "Polyvalent Nucleic Acids Nanostructures for Detection and Intracellular Gene Regulation" (2011).
105. University of Texas, Austin, TX, "Spherical Nucleic Acid Nanostructures: Establishing a New Paradigm in Materials Synthesis, Molecular Synthesis, Molecular Diagnostics, and Intracellular Gene Regulation" (2011).
106. University of Maryland, Baltimore, Translational Genomes to Personalized Medicine Symposium, Baltimore, MD, "Spherical and other Three-dimensional Forms of Nucleic Acids: A New Gene Regulation Platform" (2011).
107. Loyola University Chicago Science Week, Chicago, IL, "A Chemist's Approach to Nanofabrication: Towards a "Desktop Fab" (2011).
108. MSKCC'S Nanotechnology Center Retreat, New York, NY, "Spherical Nucleic Acid (SNA) Nanostructures: Establishing New Paradigms in Molecular Diagnostics and Intracellular Gene Regulation" (2011).

109. 11th US-Japan Symposium on Drug Delivery Systems, Maui, Hawaii, "Spherical Nucleic Acid (SNA) Nanostructures: Establishing New Paradigms in Molecular Diagnostics and Intracellular Gene Regulation" (2011).
110. NDIA for the 25th Anniversary of the MURI Program, Washington, DC; "MURI-Funded Scientific and Technological Blockbusters from Northwestern University" (2011).
111. Eindhoven University of Technology, Eindhoven, The Netherlands; "A Chemist's Approach to Nanofabrication: Towards a "Desktop Fab" (2011).
112. AFOSR Program Review, National Harbor-Oxon Hill, MD; "Dip-Pen Nanolithography Generated Combinatorial Libraries" (2011).
113. AFOSR Program Review, National Harbor-Oxon Hill, MD; "MURI: BioProgrammable One-, Two-, and Three-Dimensional Materials" (2011).

E. ADVISORY AND CONSULTATIVE FUNCTIONS

Advising

Member, President's Council of Science & Technology (PCAST, Obama Administration); American Chemical Society, Materials Research Society – Strategic Program Planning Subcommittee, American Association for the Advancement of Science, NSF Science and Technology Center for Superconductivity, Northwestern Center for Catalysis and Surface Science, Northwestern Materials Research Center, the Robert H. Lurie Cancer Center, the Nanotechnology Technical Advisory Group (nTAG), and the NSF/NIST/NIBIB Workshop: Enhancing Innovation and Competitiveness. Founding editor of Small, member of the Editorial Advisory Boards of Chemical Physics, Chemical Physics Letters, Journal of the American Chemical Society, Angewandte Chemie, Accounts of Chemical Research, Journal of Laboratory Automation, Nano Research, Advanced Materials, SENSORS, Encyclopedia of Nanoscience and Nanotechnology, Chemistry - A European Journal, Chemistry & Biology, Nanotechnology Law & Business, Journal of Materials Chemistry, Nanotech Briefs, Chemistry World of the Royal Society of Chemistry, Plasmonics, The Scientist, Journal of Scanning Probe Microscopy (JSPM), Clinical Chemistry, Nano Today, International Journal of Electrochemical Science, Nanotechnology, Science, and Applications, Nano Research, and Nanoscience and Nanotechnology. Science Advisory Board Member for the University of California Berkeley Lab Molecular Foundry and the International Society for Nanoscale Science, Computation, and Engineering. Homeland Security Innovation and Entrepreneurship Center (NU) 2005 – 2006. Member of the Board of Directors of Nanosphere and AuraSense. Member of the Iowa State University Oversight Board for the Ames Laboratory. Member of the External Advisory Board to evaluate the Clinical and Translational Science Award Program of the University of Chicago.

Consulting

Present: NanoInk, Inc., Nanosphere, Inc., Kirkland & Ellis LLP, NextGen Aeronautics, and Fuji Film, AuraSense, LLC, and AuraSense Therapeutics, LLC. Past: Pharmacia, Hexagon Packaging, Calmec Corporation, Monsanto Company, Physical Optics Corporation, and Dow Chemical Corporation

F. INVENTION DISCLOSURES/PATENTS

NU Invention No.	Invention Title	Disclosed to Government Date	Patent Application Serial No.	Patent Application Country

2009-003	Gel Pen Lithography	1/7/2009	61/153,389	United States
2009-003	Gel Pen Lithography	1/7/2009	PCT/US2010/024631	Not Applicable (PCT App)
2009-003	Gel Pen Lithography	1/7/2009	KR 10-2011-7021682	South Korea
2009-003	Gel Pen Lithography	1/7/2009	13/201,947	United States
2009-003	Gel Pen Lithography	1/7/2009	EP 10744315.2	Europe
2009-003	Gel Pen Lithography	1/7/2009	AU 2010215962	Australia
2009-003	Gel Pen Lithography	1/7/2009	JP 2011-551226	Japan
2009-003	Gel Pen Lithography	1/7/2009	CA 2,752,907	Canada
2008-162	Redox Activating Dip Pen Nanolithography (RADPN)	10/30/2008	61/116,485	United States
2008-162	Redox Activating Dip Pen Nanolithography (RADPN)	10/30/2008	61/167,852	United States
2008-162	Redox Activating Dip Pen Nanolithography (RADPN)	10/30/2008	PCT/US2009/065399	Not Applicable (PCT App)
2008-162	Redox Activating Dip Pen Nanolithography (RADPN)	10/30/2008	12/623,286	United States
2008-057	Multiplexed Dip-Pen Nanolithography with Cantilever Arrays Capable for Localizing Ink Delivered by an Ink-Jet Printer on the Tips of the Array	4/28/2008	61/047,630	United States
2008-057	Multiplexed Dip-Pen Nanolithography with Cantilever Arrays Capable for Localizing Ink Delivered by an Ink-Jet Printer on the Tips of the Array	4/28/2008	61/055,028	United States
2008-152	Curvature-Induced Base Pair "Slipping" Effects in DNA-Nanoparticle Hybridization	10/3/2008	61/108,715	United States
2008-058	Matrix-Assisted Dip-Pen Nanolithography	4/28/2008		
2010-005	Cyclopentadiene Phosphoramidite Compound and Method	1/6/2010	61/263,292	United States

	of Making Same			
2008-068	Dip-Pen Nanolithography Generated Metal Photomask	5/8/2008	61/055,055	United States
2008-068	Dip-Pen Nanolithography Generated Metal Photomask	5/8/2008	PCT/US2009/044903	Not Applicable (PCT App)
2008-173	Beam Pen Lithography	11/25/2008	61/153,400	United States
2008-173	Beam Pen Lithography	11/25/2008	PCT/US2010/024633	Not Applicable (PCT App)
2008-173	Beam Pen Lithography	11/25/2008	13/202,412	United States
2009-088	Matrix-Assisted Dip Pen Nanolithography (MA-DPN) and Matrix-Assisted Polymer Pen Lithography	5/20/2009		
2009-092	Massively Parallel Silicon Pen Nanolithography	6/10/2009	61/184,578	United States
2009-092	Massively Parallel Silicon Pen Nanolithography	6/10/2009	61/350,349	United States
2009-092	Massively Parallel Silicon Pen Nanolithography	6/10/2009	PCT/US2010/037428	Not Applicable (PCT App)
2009-092	Massively Parallel Silicon Pen Nanolithography	6/10/2009	13/375,361	United States
2009-092	Massively Parallel Silicon Pen Nanolithography	6/10/2009	EP 10784163.7	Europe
2009-092	Massively Parallel Silicon Pen Nanolithography	6/10/2009	JP- TO BE PROVIDED	Japan
2009-092	Massively Parallel Silicon Pen Nanolithography	6/10/2009	KR 10-2012-7000216	South Korea
2009-092	Massively Parallel Silicon Pen Nanolithography	6/10/2009	CA 2763907	Canada
2009-092	Massively Parallel Silicon Pen	6/10/2009	AU 2010256436	Australia

	Nanolithography			
2009-201	Guided Assembly of Sub-10 nm Single Nanoparticle Array	12/14/2009	61/265,933	United States
2009-201	Guided Assembly of Sub-10 nm Single Nanoparticle Array	12/14/2009	PCT/US2010/058715	Not Applicable (PCT App)
2009-201	Guided Assembly of Sub-10 nm Single Nanoparticle Array	12/14/2009	12/959,105	United States
2010-085	Generation of Combinatorial Patterns by Deliberate Tilting of a Polymer-Pen Array	6/30/2010	61/375,684	United States
2010-085	Generation of Combinatorial Patterns by Deliberate Tilting of a Polymer-Pen Array	6/30/2010	PCT/US2010/058773	Not Applicable (PCT App)
2011-045	Polymer Pen Lithography as a Tool for Studying Mesenchymal Stem Cell Differentiation	3/17/2011	61/453,937	United States
2011-129	Single-Molecule Protein Arrays Enabled by Scanning Probe Block Copolymer Lithography	9/27/2011	61/539,950	United States
2012-002	Positionally-defined, binary semiconductor nanoparticles synthesized by scanning probe block copolymer lithography	1/5/2012	61/583,508	United States

G. HONORS AND AWARDS

2012 ACS Award for Creative Invention
2011 Van't Hoff Prize
2011 Elected Member of the American Academy of Arts and Sciences
2011 Elected to Northwestern University Faculty and Administrator Honor Roll
2010 Elected Member of the Institute of Medicine
2010 Thomson Reuters Most Cited Chemist in the World (#1, based on total citations)
2010 Nelson W. Taylor Award, Department of Materials Science and Engineering, Penn State
2010 Elected Member of the National Academy of Sciences
2010 Herman S. Bloch Award for Scientific Excellence in Industry, University of Chicago
2010 Einstein Professorship of the Chinese Academy of Sciences (CAS)

2010 Ohio State University Edward Mack Jr. Memorial Award
2009 $500,000 Lemelson-MIT Prize
2009 Member, President's Council of Advisors on Science & Technology (PCAST, Obama Administration)
2009 Elected Member of the National Academy of Engineering
2009 Havinga Medal, Leiden University, the Netherlands
2009 Thomson Reuters Most Cited Chemist in the World (#1, total citations; #2 citations/paper)
2009 Gustavus John Esselen Award
2009 Pittsburgh Analytical Chemistry Award
2008 Biomedical Engineering Society's Distinguished Achievement Award
2008 National Security Science and Engineering Fellowship (NSSEFF) Award
2008 ACS Inorganic Nanoscience Award
2008 In Cites Top 10 Most Cited Chemists in the World (#3)